Aspects of Exciton Behavior in Amorphous Organic Thin Films

by

Conor Madigan

B.S.E. Electrical Engineering
Princeton University, 2000

SUBMITTED TO THE DEPARTMENT OF ELECTRICAL ENGINEERING AND COMPUTER SCIENCE IN PARTIAL FULFILLMENT OF THE REQUIREMENTS FOR THE DEGREE OF

MASTER OF SCIENCE IN ELECTRICAL ENGINEERING AND COMPUTER SCIENCE
AT THE
MASSACHUSETTS INSTITUTE OF TECHNOLOGY

May 2002

Signature of Author:_____
Department of Electrical Engineering and Computer Science
May 24, 2002

Certified by:_____
Vladimir Bulović
Professor of Electrical Engineering and Computer Science
Thesis Supervisor

Accepted by:_____
Arthur C. Smith
Chairman, Department Committee on Graduate Students

Aspects of Exciton Behavior in Amorphous Organic Thin Films

by

Conor Madigan

Submitted to the Department of Electrical Engineering and Computer Science in Partial Fulfillment of the Requirements for the Degree of Master of Science in Electrical Engineering and Computer Science

ABSTRACT

In this thesis we report two experimental phenomena which shed new light onto the behavior of excitons in amorphous organic thin films. First, we report a controllable shift in the photoluminescence of the red laser dye DCM2 from 563 nm to 605 nm in thin films of polystyrene (PS) and camphoric anhydride (CA) by modification of the film CA concentration. Measurements of the film electronic susceptibility, ε, reveal that increasing the CA concentration markedly increases ε, and we show that the spectral shift in DCM2 can be attributed to a simple solvation phenomenon, as observed for many years in liquids. We find that such "solid state solvation" should operate in the entire class of amorphous organic solids, and play a major role in determining absorption and emission spectra. The potential effect of permanent, internal local fields is also described.

Second, we report the experimental measurement of dynamic spectral red shifts in the photoluminescence of thin films of Aluminium Tris(8-hydroxylquinoline) (Alq_3) doped with the red laser dye DCM2. These spectral shifts (in terms of the difference between final and initial peak energies) have an average magnitude of ~ 0.08 eV over a time window of ~ 4 ns, for dopings ranging between 0.5% and 4.7%. We show that this previously unreported phenomenon can be attributed to the diffusion of excitons through the film by means of Forster energy transfer between DCM2 molecules. We present a theoretical model detailing this mechanism and a Monte-Carlo simulation of the process. We find that the simulation results are consistent with the experimentally observed data, and that the technique provides a sensitive probe of the Forster radius and the excitonic density of states. The impact on these results of doping density variations, which are common in doped, small molecule organic thin films, is also described.

Thesis Supervisor: Vladimir Bulović
Title: Professor of Electrical Engineering and Computer Science

CONTENTS

SYMBOL LEGEND

V	**an electrical potential operator**
H	**a Hamiltonian**
E	**energy associated with a particular Hamiltonian**
$\|\Psi\rangle$	**wavefunction solution to Time Dependant Schrödinger Equation (TDSE)**
$\|\psi\rangle$	**spatial wavefunction solution to Time Independant Schrödinger Equation (TISE)**
$\|\theta\rangle$	**temporal wavefunction solution associated with TISE**
V_{ee}	**electron-electron interaction potential in molecular Hamiltonian**
V_{nn}	**nucleus-nucleus interaction potential in molecular Hamiltonian**
V_{en}	**electron-nucleus interaction potential in molecular Hamiltonian**
H_{el}	**electronic Hamiltonian under Born-Oppenheimer approximation**
H_{nucl}	**nuclear Hamiltonian under Born-Oppenheimer approximation**
E_{el}	**electronic energy under Born-Oppenheimer approximation**
$\|\psi_{el}\rangle$	**electronic wavefunction under Born-Oppenheimer approximation**
$\|\psi_{nucl}\rangle$	**electronic wavefunction under Born-Oppenheimer approximation**
$\|G\rangle$	**ground state, equilibrium molecular wavefunction**
$\|E\rangle$	**lowest energy exciton state, equilibrium molecular wavefunction**
$\|g\rangle$	**ground state, equilibrium electronic wavefunction**
$\|e\rangle$	**lowest energy excited state, equilibrium electronic wavefunction**
$\Uparrow$	**a generic spin up wavefunction**
$\Downarrow$	**a generic spin down wavefunction**
ω	**an angular frequency (in radians/second)**
ν	**an angular frequency (in hertz)**
μ	**a dipole moment (in debyes)**
$\Gamma_{total}^{\uparrow}$	**molecular absorption transition rate (in 1/second)**
$\Gamma_{total}^{\downarrow}$	**molecular emission transition rate (in 1/second)**
ε	**bulk electronic susceptibility (no units in cgs)**
$\vec{F}$	**an electric field**
ρ	**a density of states**
φ	**an electronic potential function**
c	**speed of light**
Γ_F	**Forster transition rate**
Γ_D	**Dexter transition rate**
S_D	**normalized donor emission spectrum**
σ_A	**normalized acceptor absorption cross section (in cm^2)**

R_F **Forster radius**

$\widetilde{R}_F$ **effective Forster radius**

η **radiative quantum yield (a.k.a. radiative quantum efficiency)**

τ_{rad} **radiative lifetime**

τ **observed radiative lifetime**

ΔE_{solv} **energy shift due to solvation**

ΔE_{static} **energy shift due to static fields**

1. INTRODUCTION AND BACKGROUND

1.1 Introduction

Over the last two decades interest in the optoelectronic properties of amorphous organic thin films has risen dramatically, due to their potential application in devices such as light emitting diodes, solar cells, photodetectors, and lasers [1-4]. As a result, it has become increasingly important that we understand the physics underlying optoelectronic processes in such systems. For organic materials in this field, the exciton has remained the fundamental optoelectronic excitation of interest, and in this thesis we further develop the theory of excitons in amorphous organic solids.

In the context of this paper, an exciton describes a molecular excitation in which a single electron is displaced from one of the orbitals occupied in the ground state into one of the orbitals unoccupied in the ground state. An exciton can be equivalently viewed as a bound electron-hole pair (where the hole refers to the electronic state just vacated by the excited electron). There are many possible excitons, depending on which molecular orbitals are occupied by the excited electron and hole respectively reside. However, in the vast majority of cases only the lowest energy exciton is of importance. The formation of this exciton involves the excitation of an electron from the highest occupied molecular orbital (HOMO) to the lowest unoccupied molecular orbital (LUMO).

Such excitons can be formed by the absorption of a photon (of sufficient energy) or by the meeting of an electron and a hole on the same molecule. In this thesis we are only concerned with the former formation process, which we refer to as optical excitation. (The latter is referred to as electrical excitation.) Once the exciton has formed, there are a number of possibilities. First, the exciton can relax emissively, in which case it emits a photon with energy corresponding to the exciton energy. Second, the exciton can relax non-emissively, in which case it transfers its energy into phonons (and locally heats the solid). Third, the exciton can dissociate, in which case an electron (hole) will be left behind on that molecule and a hole (electron) created on some nearby molecule. Finally, the exciton can move to another molecule,

by some kind of energy transfer mechanism. All of these processes contribute to the behavior of existing organic optoelectronic devices.

Therefore, to understand how such devices operate, we must understand nature of excitons in amorphous organic solids: we must know how they are created, how they behave over the course of their lifetime, and how they are destroyed. At first this might seem like a simple problem. We could simply begin with first principles and describe the problem in terms of the appropriate Hamiltonian for the molecule in question and all the surrounding molecules with which it interacts. Then we could solve this Hamiltonian to determine the desired molecular states, and since the original Hamiltonian would have in principle contained all the physics, the problem at that point, would be done. With the relevant molecular states determined, one could compute any experimentally measurable property that one desired.

Unfortunately, when dealing with amorphous molecular solids we are faced with a situation where strong intermolecular interactions are present—after all, it is due to such interactions that the material forms a condensed phase in the first place—but no long range order exists. Because of the former, the Hamiltonian must include terms dealing with a large number of molecules, but because of the latter, one can not invoke any of the group theory (developed by the solid state physics community) used to simplify computations of large numbers of interacting atoms. As a result, in the absence of serious approximations, first principles treatments of this nature are not (yet) computationally feasible.

One need not be able to perform *ab initio* calculations, however, to have a useful understanding of excitons in amorphous organic solids. Indeed, resorting to such calculations exclusively could obscure the essential physical processes involved. Rather we could start by first considering the behavior of isolated molecules and then attempting to identify the specific ways in which the properties of these isolated molecules would be altered in the solid state. In this thesis we present experimental results which allow us to better understand the behavior of excitons in amorphous organic solids, providing a starting point for the development of a general theory applicable to all disordered molecular solids.

For the remainder of this section we review the basic physics of excitons. In Section 2 we turn to the topic of local field effects on exciton energies. We review the physics underlying such effects, and also present experiment results that demonstrate the phenomenon of solid state

solvation, one of the main mechanisms by which exciton energies are modified in the solid state. In Section 3 we address the process of Forster energy transfer, by which excitons can diffuse through a solid. We present experimental results which measure the dynamics of this process, along with a detailed simulation of the phenomenon. By varying the simulation parameters to properly fit the data, we can probe such critical properties of our materials as the Forster radius and the excitonic density of states. Finally, in Section 4, we review our findings and identify how this work can be extended to yield yet further insights into exciton behavior in amorphous organic solids.

1.2 The Molecular State of an Exciton

We begin by describing excitons on isolated molecules, which corresponds practically to the case of molecules in the gas phase. For an isolated molecule, fairly sophisticated ab initio computations *are* possible with modern techniques, and it is useful to begin from first principles.

We begin with a single particle system, for which the general Hamiltonian is simply,

$$H = -\frac{\hbar^2}{2m}\nabla^2 + V(\vec{r},t) \tag{1}$$

where m is the particle mass, and $V(\vec{r},t)$ is the potential function operating on the particle. (See e.g. [5,6] for good reviews of quantum mechanics.) To obtain the set of wavefunctions, $\{|\Psi\rangle\}$, describing the allowed states of the system, we solve the Time-Dependant Schrödinger Equation (TDSE),

$$i\hbar\frac{\partial}{\partial t}|\Psi\rangle = H|\Psi\rangle = \left[-\frac{\hbar^2}{2m}\nabla^2 + V(\vec{r},t)\right]|\Psi\rangle . \tag{2}$$

The $\{|\Psi\rangle\}$ in principle provide us with all the physics of the system. Their squared magnitude (i.e. $|\Psi|^2$) describes the probability distribution for finding that particle at any given point in space. With the $\{|\Psi\rangle\}$ we can also obtain any observable (i.e. measureable quantity) o from,

$$o = \int \Psi^* \hat{O} \Psi d^3r \Leftrightarrow \langle\Psi|\hat{O}|\Psi\rangle$$

where $\hat{O}$ is the operator associated with the desired observable. In general, the $\{|\Psi\rangle\}$ are all functions of both space and time.

Even when considering a single atom (never mind the collection of atoms comprising a molecule), the TDSE presents a mathematically intractable problem, leading us to make an immediate simplification. Instead of considering a fully time-dependant problem, we instead consider only a time-independent one; in other words, we only consider the case of $V(\vec{r},t)=V(\vec{r})$. This simplification allows us to separate the time and space dependant parts of the Hamiltonian in the following way. First, we assume the following form for $|\Psi(\vec{r},t)\rangle$,

$$|\Psi(\vec{r},t)\rangle = |\psi(\vec{r})\rangle|\theta(t)\rangle$$

which when plugged into equation (2) yields,

$$i\hbar|\psi\rangle\frac{\partial}{\partial t}|\theta\rangle = -\frac{\hbar^2}{2m}|\theta\rangle\nabla^2|\psi\rangle + V(\vec{r})|\theta\rangle|\psi\rangle$$

If we then divide by $|\psi\rangle|\theta\rangle$ we get,

$$i\hbar\frac{1}{|\theta\rangle}\frac{\partial}{\partial t}|\theta\rangle = -\frac{\hbar^2}{2m}\frac{1}{|\psi\rangle}\nabla^2|\psi\rangle + V(\vec{r}).$$

Since the left side is only dependant on time and the right side is only dependant on space, varying time can only vary the left side, while varying space can only vary the right side. Therefore, for the left and right to remain equal, they must be constant. This constant is in fact the energy of the system, and we denote it by E. Setting each side separately equal to E yields the following two differential equations,

$$i\hbar\frac{\partial}{\partial t}|\theta\rangle = E|\theta\rangle$$

$$\left[-\frac{\hbar^2}{2m}\nabla^2 + V(\vec{r})\right]|\psi\rangle = E\psi \tag{3}$$

the second of which is known as the Time-Independent Schrödinger equation (TISE). The associated time-independent Hamiltonian is trivially extracted from (3),

$$H = -\frac{\hbar^2}{2m}\nabla^2 + V(\vec{r}). \tag{4}$$

From the TISE, we can make the leap to a many particle problem, and write down the full Hamiltonian for the general molecular system:

$$H = -\sum_{i=1}^{N} \frac{\hbar^2}{2m_e} \nabla_i^2 + -\sum_{A=1}^{M} \frac{\hbar^2}{2m_A} \nabla_A^2 + V_{ee} + V_{nn} + V_{en} \tag{5}$$

where

$$V_{ee} = \frac{e^2}{4\pi\varepsilon_0} \sum_{i=1}^{N} \sum_{j>i}^{N} \frac{1}{\left|\vec{r}_i - \vec{r}_j\right|}$$

$$V_{nn} = \frac{e^2}{4\pi\varepsilon_0} \sum_{A=1}^{M} \sum_{A>B}^{M} \frac{Z_A Z_B}{\left|\vec{R}_A - \vec{R}_B\right|}$$

$$V_{en} = -\frac{e^2}{4\pi\varepsilon_0} \sum_{i=1}^{N} \sum_{A=1}^{M} \frac{Z_A}{\left|\vec{r}_i - \vec{R}_A\right|}.$$

In (5), the first term describes the kinetic energy of the electrons, the second term describes the kinetic energy of the nuclei, the third term describes the electronic coulomb repulsion, the fourth term describes the nuclear coulomb repulsion, and the final term describes the electron-nucleus coulomb attraction. (See e.g. [7,8] for treatments of the molecular quantum mechanical problem.) This general expression describes a system of N electrons (each with mass m_e) and M nuclei (where the A'th nucleus has mass m_A). In such a system, there are N+M different particles, and therefore there are N+M separate coordinates; in other words, $|\psi\rangle = \left|\psi\left(\vec{r}_1, \cdots, \vec{r}_N, \vec{R}_1, \cdots, \vec{R}_M\right)\right\rangle$, where in this construction, the N $\vec{r}$ coordinates are associated with the electrons, and the M $\vec{R}$ coordinates are associated with nuclei. The gradient operators in (5) operate only on the coordinate associated with their subscript, such that ∇_i^2 operates on $\vec{r}_i$ and ∇_A^2 operates on $\vec{R}_A$. As explained above, we have assumed that the potential function is not time-dependant in obtaining the TISE. Since in the molecular problem V is determined by the positions of the various particles in the system then the solutions to (5) clearly describe the states of the molecule in which all the particles in the system are in equilibrium. If they were not in equilibrium, they would not be static, and therefore V would be time-dependant, which is explicitly forbidden in a time-*in*dependent treatment.

The TDSE in (5) is still too complex to treat exactly for all but the simplest systems, and we now apply the so-called Born-Oppenheimer approximation to proceed. In applying this approximation, we argue that since the nuclei are so much heavier than the electrons, they move much more slowly. Therefore, we can think of the electrons as being capable of instantaneously responding to changes in the nuclear positions. As a result, we can solve the electronic part of our Hamiltonian under the assumption that the nuclei are stationary. Within this assumption, the term in (5) due to the kinetic energy of the nuclei is zero, and V_{nn} is a constant (so we can temporarily drop it too, since it simply shifts E without affecting the $|\psi\rangle$). This leaves us with an electronic Hamiltonian of,

$$H_{el} = -\sum_{i=1}^{N} \frac{\hbar^2}{2m_e} \nabla_i^2 + V_{ee} + V_{en}. \tag{6}$$

and the associated eigenvalue problem,

$$H_{el}|\psi_{el}\rangle = E_{el}|\psi_{el}\rangle.$$

To solve this now purely electronic problem we need only deal directly with the electronic coordinates $\vec{r}$. The $|\psi_{el}\rangle$ still have an implicit dependence on the nuclear coordinates since changing the nuclear coordinates changes H_{el}, but the differential equation does not need to treat these coordinates as free variables, making the problem mathematically much simpler.

Of course, the nuclear problem has not disappeared. But we note that if the electrons are assumed to be moving much faster than the nuclei, then the nuclei only see their average behavior, and we get a nuclear Hamiltonian of,

$$\begin{aligned} H_{nucl} &= -\sum_{A=1}^{M} \frac{\hbar^2}{2m_A} \nabla_A^2 + V_{nn} + \langle H_{el} \rangle \\ &= -\sum_{A=1}^{M} \frac{\hbar^2}{2m_A} \nabla_A^2 + V_{nn} + E_{el}\left(\vec{R}_1, \cdots, \vec{R}_M\right) \end{aligned} \tag{7}$$

with the associated eigenvalue problem,

$$H_{nucl}|\psi_{nucl}\rangle = \varepsilon|\psi_{nucl}\rangle.$$

As a result, under the Born-Oppenheimer approximation, the differential equations dealing with the electronic and nuclear coordinates are decoupled. We find the solution by first solving the

electronic problem, which gives us the $\{|\psi_{el}\rangle\}$ and $\{E_{el}\}$ that describe the various physically allowed electronic states. Then we plug into (7) the E_{el} corresponding to the electronic state of interest and solve the nuclear problem. When solving the nuclear problem, V_{nn} and $E_{el}(\vec{R}_1,\cdots,\vec{R}_M)$ can be thought of as together comprising the potential within which the nuclei reside. The total wavefunction, $|\psi\rangle$, in the Born-Oppenheimer approximation is just $|\psi_{nucl}\rangle|\psi_{el}\rangle$.

The most fundamental molecular state is the equilibrium ground state, which is the state with the lowest total energy. This state also serves as our starting point in discussing excitations, for it is in reference to this ground state that our excitations are defined. Electronic excited states for which there is no change in the number of particles in the system are called excitons, and as discussed above, we are interested in the lowest energy such excitation. We can identify it by finding the state with the second lowest value for the *electronic* energy, E_{el}, and the associated $|\psi_{el}\rangle$. Since the specification of an exciton only defines the electronic arrangement of the molecules, any choice of $|\psi_{nucl}\rangle$ is valid, so long as $|\psi_{el}\rangle$ still describes the state with the second lowest value for the E_{el}. Strictly speaking, which electronic state corresponds to the ground and first excited state need not be unique to all nuclear positions, and therefore to all $|\psi_{nucl}\rangle$. However, in this thesis, we can assume that the ground and first excited electronic states always correspond to the same states for all physically reasonable $|\psi_{nucl}\rangle$. As a result, we will not worry about $|\psi_{nucl}\rangle$ when defining the electronic component of the exciton state.

To set up the discussion that follows, we identify the equilibrium molecular ground state by $|G\rangle$ and our equilibrium molecular exciton state by $|E\rangle$. It is also useful to identify the $|\psi_{el}\rangle$ associated with each of these states as $|g\rangle$ and $|e\rangle$ respectively. The electronic wavefunctions are called molecular orbitals in the common vernacular, and $|g\rangle$ and $|e\rangle$ are simply the HOMO and LUMO levels alluded to earlier.

Before leaving the quantum mechanical development of our molecular electronic states behind for good, we turn to one final issue: spin. In the above, no explicit mention of spin was made. However, we know that the molecular orbitals must include a spin component if they are

to adequately describe a full electronic state. So we say that the $\{|\psi_{el}(\vec{r})\rangle\}$ are really *spin* orbitals and have either up or down spin character. Furthermore, we know that each electronic level can hold two electrons, one with spin up and one with spin down. As we will see presently, spin plays an important role in the description of an exciton.

In the vast majority of cases, we are dealing with a molecule in which all of the electrons are paired in the ground state. (Molecules with this property are sometimes referred to as "closed.") In this case, the excitonic state includes two unpaired electrons, one in the HOMO and one in the LUMO. The importance of this is that in a system of two particles with spin, we are constrained by quantum mechanics to form states with total spin 0 or 1. If we represent a spin-up state by $\Uparrow$ and a spin-down state by $\Downarrow$, and denote our two particles as 1 and 2 respectively, we find that we can get three orthogonal total spin 1 states, given by,

$$\Uparrow(1)\Uparrow(2)$$

$$\frac{1}{\sqrt{2}}\left(\Uparrow(1)\Downarrow(2)+\Downarrow(1)\Uparrow(2)\right)$$

$$\Downarrow(1)\Downarrow(2)$$

and one orthogonal total spin 0 state, given by,

$$\frac{1}{\sqrt{2}}\left(\Uparrow(1)\Downarrow(2)-\Downarrow(1)\Uparrow(2)\right).$$

These four orthogonal functions completely define the two-particle spin-space. Because states made up of a combination of both the spin 0 and spin 1 states are disallowed (because they would have a total spin between 0 and 1), we realize that our exciton is either in the single spin 0 state, or it is comprised of some combination of the spin 1 states. These two types of excitons are fundamentally different, and in accordance with their respective multiplicities, the total spin 1 excitons are referred to as triplets, and the total spin 0 excitons as singlets.

In some cases, the spin of the electrons in a molecule are strongly coupled to other angular momenta in the molecule (usually their own orbital angular momentum, but sometimes that of the surrounding nuclei), and the total spin ceases to be a good quantum number. Then one must consider the fully coupled system and look at the total angular momentum instead. In such cases, excitons can be formed with both singlet and triplet character.

1.3 Exciton Creation and Annihilation – State Energies

We have laid down the basic quantum mechanical groundwork that we require to understand the essential physics of excitons, and now turn to the task of determining the creation and annihilation energies of an exciton. Before we do this, we must first differentiate between excitons formed by optical and electrical excitations. When an exciton is formed by the absorption of a photon, the total electronic spin of the system remains unchanged (because photons can not contribute or remove spin). For a closed system, the total electronic spin is always 0, and so an exciton formed by the absorption of a photon will also always have spin 0. Therefore, when the ground state is a singlet, only singlet excitons are created by optical excitations. Conversely, when the exciton is formed by the meeting of an electron and a hole on the same molecule, the spins of the two unpaired electrons are uncorrelated, and both singlets and triplets can be formed. While such electrically excited excitons play a critical role in organic optoelectronic devices, as we have noted above, in this thesis we are only concerned with optically excited excitons. (As noted in the previous section, in some materials, the singlet-triplet distinction does not hold. In such cases, one can optically excite an exciton that is primarily singlet in character, but which can become primarily triplet in character over time. While this phenomenon is critical in a number of important organic optoelectronic systems, in this thesis we will not be dealing with this situation.)

To compute the energy to optically generate an exciton, one must recall the Born-Oppenheimer approximation to determine the energy associated with the creation of the excited state. Earlier we argued that electrons move much more quickly than nuclei (a concept also known as the Franck-Condon principle). As a result, when discussing electronic excitations, we are really describing excitations that are created within a fixed nuclear framework. Therefore the energy required to create an exciton corresponds to the difference in the energy between the excited and ground electronic states *with the nuclei positioned in equilibrium with the electronic ground state*. So the energy for creating an exciton is *not* in fact the difference in energy between the equilibrium ground and excited molecular states. Generally speaking, the nuclei subsequently have enough time to achieve equilibrium with the electronic excited state before the exciton is destroyed, and as a result, the energy released in destroying an exciton is given by

the difference between the excited and ground electronic states *with the nuclei positioned in equilibrium with the electronic excited state.*

This is illustrated schematically in Figure 1.1. The vertical scale reflects energy, while the horizontal scale is a generalized "nuclear coordinate," which can be thought of as simply a parameterized line of nuclear coordinates connecting the equilibrium ground and excited nuclear configurations. The most important point to grasp here is that the minimum energy for the electronic ground state and the electronic excited state need not correspond to the same nuclear coordinates. Following the Franck-Condon principle we represent electronic transitions as vertical lines. If we follow the sequence of events illustrated in the diagram, then first we excite an electron from the minimum of the ground state (i.e we create the exciton). Over time, the system relaxes to a new set of nuclear coordinates that minimizes the energy of the system in the excited state. Once the system has fully relaxed in the excited state, the electron relaxes back to the ground state (i.e. we destroy the exciton). Over time, the system again relaxes to a new set of coordinates, now such that the energy of the system in the ground state is minimized. The remarkable property of this system is that the excitation and relaxation energies of the exciton are different. This energetic difference, first observed as a shift in the center wavelength of gas phase absorption and fluorescence spectra, is known as the Franck-Condon shift.

This phenomenon can be straightforwardly integrated into our quantum development, despite the fact that by starting with the TISE we technically limited ourselves to the determination of equilibrium states. In short, since $|g\rangle$ and $|e\rangle$ are implicitly dependant on the nuclear coordinates, if we have determined them in the first place, then we know their (and their associated energy's) dependence on the nuclear coordinates. Furthermore, in determining $|G\rangle$ and $|E\rangle$ we determine the equilibrium nuclear coordinates in the ground and excited states, which we define as $\vec{R}_G$ and $\vec{R}_E$ respectively. With these definitions, we can describe the four different states involved in the creation and destruction of our exciton,

$$1: \left|g\left(\vec{R}_G\right)\right\rangle, E_g\left(\vec{R}_G\right) \Leftrightarrow |g\rangle, E_g$$

$$2: \left|e\left(\vec{R}_G\right)\right\rangle, E_e\left(\vec{R}_G\right) \Leftrightarrow |e^*\rangle, E_e^*$$

$$3: \left|e\left(\vec{R}_E\right)\right\rangle, E_e\left(\vec{R}_E\right) \Leftrightarrow |e\rangle, E_e$$

$$4: \left|g\left(\vec{R}_E\right)\right\rangle, E_g\left(\vec{R}_E\right) \Leftrightarrow \left|g^*\right\rangle, E_g^*$$

where the sense of the shorthand is that the asterisk denotes the non-equilibrium state. These are the four states identified in Figure 1.1. (Note that state 1 is just $|G\rangle$ and state 3 is just $|E\rangle$.)

1.4 Exciton Creation and Annihilation – Transition Rates

We now understand the energies involved in creating and destroying our exciton but we have not discussed yet the actual transitions themselves. Since these processes describe changes to the molecular system, they do not fall under the purview of a static, or time-independent picture, which forces us to employ a time-dependant approach. Fortunately, perturbation theory allows us to treat the problem without having to go back to the beginning. The basic premise of time-dependant perturbation theory is that the states of the system are not strongly affected by the perturbing potential, and that the primary contribution of the potential is to induce transitions between different states. (In this section we follow the time-dependant perturbation theory development in [6].)

We begin by writing down the Hamiltonian of the perturbed system as,

$$H = H_0 + V(t) = H_0 + \lambda \tilde{V}(t) \tag{8}$$

where H_0 is the Hamiltonian of the unperturbed system, and note that the objective of our analysis is to determine the probability of finding the system in state $|f\rangle$ at time t after being in state $|i\rangle$ at time $t = 0$. The $V(t)$ is assumed to be small compared to H_0. To formalize this, we express $V(t)$ as $\lambda \tilde{V}(t)$, where $\tilde{V}(t)$ is of the same order as H_0 but $\lambda << 1$. Since we will be treating the potential as a perturbation, we start by solving the unperturbed, time-independent problem,

$$H_0|n\rangle = E_n|n\rangle \tag{9}$$

for the $|n\rangle$ and E_n. We then turn to the general problem of solving the TDSE,

$$i\hbar \frac{\partial}{\partial t}|\Psi(t)\rangle = \left[H_0 + \lambda \tilde{V}(t)\right]\Psi(t)\rangle \tag{10}$$

with the initial condition,

$$|\Psi(t)\rangle = |i\rangle.$$

The starting point of the method is to assume that,

$$|\Psi(t)\rangle = \sum_n c_n(t)|n\rangle \tag{11}$$

which, we note, does not represent an approximation since the set of $|n\rangle$ comprise an orthogonal basis for the entire space. As we will see, the approximation only arises in our calculation of the $c_n(t)$.

By left multiplying (11) with $\langle n|$ we see that,

$$c_n(t) = \langle n|\Psi(t)\rangle. \tag{12}$$

From (9) we have that,

$$\langle k|H_0|n\rangle = E_n\delta_{nk}. \tag{13}$$

We also introduce the shorthand,

$$\langle k|\tilde{V}(t)|n\rangle = \tilde{V}_{nk}. \tag{14}$$

Using these relationships, we see that by inserting (11) into (10) and left multiplying by $\langle k|$, we get,

$$i\hbar\frac{d}{dt}c_n(t) = E_n c_n(t) + \lambda\sum_k \tilde{V}_{kn}c_k(t). \tag{15}$$

Since we are assuming that the perturbing potential is small, we might be able to simplify the problem by assuming that part of the time dependence of the $c_n(t)$ is the time dependence of the unperturbed system. If we let $\lambda \to 0$, then,

$$c_n(t) \to b_n e^{-iE_n t/\hbar}$$

so, we propose that,

$$c_n(t) = b_n(t)e^{-iE_n t/\hbar}. \tag{16}$$

Plugging (16) into (15) and rearranging we get,

$$i\hbar\frac{d}{dt}b_n(t) = \lambda\sum_k e^{i\omega_{nk}t}\tilde{V}_{kn}(t)b_k(t) \tag{17}$$

where

$$\omega_{nk} = \frac{E_n - E_k}{\hbar}.$$

To obtain our coefficients, we then must, in principle, solve (17).

To proceed, we now assume a power series expansion in λ for the $b_n(t)$,

$$b_n(t) = b_n^{(0)}(t) + \lambda b_n^{(1)}(t) + \lambda^2 b_n^{(2)}(t) + \cdots. \tag{18}$$

If we plug (18) into (17) and then separately equate the coefficients of λ^r we have for $r = 0$,

$$i\hbar \frac{d}{dt} b_n^{(0)}(t) = 0 \tag{19}$$

and for $r \neq 0$,

$$i\hbar \frac{d}{dt} b_n^{(r)}(t) = \sum_k e^{i\omega_{nk}t} \tilde{V}_{kn}(t) b_k^{(r-1)}(t). \tag{20}$$

We obtain the first order solutions from (19) and the initial conditions. Immediately we see that $b_n^{(0)}(t) = b_n^{(0)}$ (i.e. there is no time-dependance) and therefore the initial conditions trivially determine the $b_n^{(0)}$. For our initial conditions,

$$b_n^{(0)} = \begin{cases} 1 & n = i \\ 0 & n \neq i \end{cases}.$$

From (20) we can then obtain the r'th solution from the (r-1)'th solution. To obtain the first order, we must then solve,

$$i\hbar \frac{d}{dt} b_n^{(1)}(t) = \sum_k e^{i\omega_{nk}t} \tilde{V}_{kn}(t) b_k^{(0)} = e^{i\omega_{ni}t} V_{in}(t)$$

which means that,

$$b_n^{(1)}(t) = \int_o^t e^{i\omega_{ni}t'} \tilde{V}_{in}(t') dt'.$$

The probability of finding a system in a state $|2\rangle$ at time t after starting in state $|1\rangle$ at $t = 0$, $P_{21}(t)$, is given by the squared magnitude of the wavefunction overlap of the two states,

$$P_{fi}(t) = \left| \langle 2|1 \rangle \right|^2.$$

So to compute the transition probability that is the goal of this analysis, we need to express $|1\rangle$ and $|2\rangle$ for our problem. By construction, state $|2\rangle$ is just the unperturbed $|f\rangle$. State $|1\rangle$ is the time-evolving perturbed state that we have been solving for, and to first order, it is just,

$$|1\rangle = |i\rangle + \lambda \sum_k b_k^{(1)}(t)|k\rangle$$

so our transition probability to first order is,

$$P_{fi}(t) = \lambda^2 \left|b_f^{(1)}(t)\right|^2 = \frac{1}{\hbar^2}\left|\int_0^t e^{i\omega_{fi}t'} V_{fi}(t')dt'\right|^2 \tag{20}$$

where in the last step we have reintroduced the true potential $V(t)$.

If we take $V(t)$ to have the form of a sinusoidal perturbation, as appropriate for a radiation field,

$$V(t) = V\cos\omega t = V\frac{\left(e^{i\omega t} + e^{-i\omega t}\right)}{2}$$

then we can evaluate the integral in (20) to get,

$$P_{fi}(t) = \frac{|V_{fi}|^2}{4\hbar^2}\left|\frac{1-e^{i(\omega_{fi}+\omega)t}}{\omega_{fi}+\omega} + \frac{1-e^{i(\omega_{fi}-\omega)t}}{\omega_{fi}-\omega}\right|^2$$

$$= \frac{|V_{fi}|^2}{\hbar^2}\frac{\left|e^{i\omega_{fi}t}-1\right|^2}{\omega^2}$$

$$= \frac{|V_{fi}|^2}{\hbar^2}\left[\frac{\sin(\omega_{fi}t/2)}{\omega_{fi}t/2}\right]^2.$$

To now connect this to the absorption and emission processes, we realize that the radiation field itself constitutes a part of our "system." In short, when we describe absorption, we mean not only a change in state of the molecule but also a change in state of the surrounding radiation field. For absorption, the change in the radiation field involves the removal of a photon from an existing field. For emission, the change in the radiation field involves the addition of photon to the vacuum (or zero) radiation field. This latter case actually creates a problem for a semi-classical treatment, because for emission (by which we mean spontaneous emission), there

is no field initially present, and therefore no perturbing potential. If we introduced the radiation field formally, using quantum electrodynamics, we could treat the problem without difficulty, but this requires the quantization of the radiation field and the introduction of a number of new operators (see e.g. [9]). To avoid this we proceed with a semi-classical development of the absorption rate, and at the end we will follow Einstein's argument to derive the emission rate (as done in [7]).

To proceed with obtaining the absorption rate with a semi-classical method, we note that in the absorption process any degenerate final states with the proper molecular electronic arrangement are equivalent, and so we must account for transitions into all of the possible final radiation field states. Since the radiation field is given by a continuum of states, this requires integrating over some density of states function. In other words,

$$P_{total}(t) = \int_{\omega_{fi}-\Delta\omega/2}^{\omega_{fi}+\Delta\omega/2} \frac{|V_{fi}|^2}{\hbar}\left[\frac{\sin\left((\omega_{fi}-\omega)t/2\right)}{(\omega_{fi}-\omega)t/2}\right]^2 \rho(\hbar\omega)d\omega \tag{21}$$

where $\Delta\omega$ defines the energy uncertainty, $\hbar\Delta\omega$, of our final state, $\rho(\hbar\omega)$ is the density of states of the radiation field, and we assume that the final state energy is centered around $\hbar\omega_{fi}$. In obtaining (21), we have noted that since $\rho(\hbar\omega)$ is really defined in terms of energy,

$$\rho(E)dE = \hbar\rho(\hbar\omega)d\omega,$$

yielding an extra factor of $\hbar$. In general we can assume that $\rho(\hbar\omega)$ should be slowly varying with ω near ω_{fi} compared to,

$$\left[\frac{\sin(\omega_{fi}t/2)}{\omega_{fi}t/2}\right]^2,$$

so we take it to be approximately constant at its value at $\omega = \omega_{fi}$. This allows us to write (21) as,

$$P_{total}(t) = \frac{|V_{fi}|^2}{\hbar}\rho_{fi}\int_{\omega_i-\Delta\omega/2}^{\omega_i+\Delta\omega/2}\left[\frac{\sin(\omega_{fi}t/2)}{\omega_{fi}t/2}\right]^2 d\omega_f = 2\frac{|V_{fi}|^2 t}{\hbar}\rho_{fi}\int_{-t\Delta\omega/4}^{t\Delta\omega/4}\left[\frac{\sin(x)}{x}\right]^2 dx$$

where $\rho_{fi} \equiv \rho(\omega = \omega_{fi})$. For times sufficiently large that,

$$t\Delta\omega >> 1$$

we can approximate the boundaries of integration as $\pm\infty$, and since

$$\int_{-\infty}^{\infty}\left[\frac{\sin(x)}{x}\right]^2 dx = \pi$$

this then gives,

$$P_{total}(t) = \frac{2\pi}{\hbar}\rho_{fi}\left|V_{fi}\right|^2 t\,.$$

Differentiating with time, we get the associated transition rate, Γ_{total},

$$\Gamma_{total} = \frac{2\pi}{\hbar}\rho_{fi}\left|V_{fi}\right|^2 \tag{22}$$

which is just Fermi's Golden Rule, and applies generally to any transition rate in which the final state is part of a continuum with state density at ω_{fi} given by ρ_{fi}. Although we have made some approximations in obtaining this expression, it holds for a surprisingly broad set of conditions. We can reasonably assume its validity in our development of absorption and emission, though precise calculations would involve, for instance, more than just the first order component of the time-dependant perturbation solution.

In the semi-classical treatment, if the wavelength of radiation, and spatial variation of the field intensity, is much larger than the size of the molecule, then we can operate in the so-called electric dipole approximation. In this case, the radiation field interacts with the molecule through the transition dipole, which is the difference between the ground and excited state dipoles. Specifically, the interaction Hamiltonian is given by,

$$V = -\vec{F}\cdot\hat{\mu}$$

where $\vec{F}$ is the radiation field vector at the center of mass of the molecule and $\hat{\mu}$ is the molecular dipole operator. For this kind of interaction,

$$\Gamma_{total} = \frac{2\pi}{\hbar}\rho_{fi}\mu_{fi}^2 F^2\gamma^2 \tag{23}$$

where γ is the normalized dot product of $\vec{\mu}_{fi}$ with the radiation field, i.e.,

$$\gamma = \frac{\vec{\mu}_{fi}\cdot\vec{F}}{\left|\vec{\mu}_{fi}\right|\left|\vec{F}\right|}.$$

For the absorption process, ρ_{fi} is determined experimentally, i.e. one supplies a particular density of photons, and this defines the density of radiation states. To obtain a more useful form for (23) we first identify the volume energy density of the field, ζ,

$$\zeta = 2\varepsilon_0 F^2.$$

With this definition,

$$\Gamma_{total} = \frac{\pi}{\varepsilon_0 \hbar} \mu_{fi}^2 \gamma^2 (\zeta \rho_{fi}).$$

Then if we define a radiative energy density of states, $\rho_{rad}(\omega)$, such that,

$$\zeta \rho_{fi} \hbar d\omega = \rho_{rad}(\omega_{fi}) d\omega$$

we get that,

$$\Gamma_{total} = \frac{\pi}{\varepsilon_0 \hbar^2} \mu_{fi}^2 \gamma^2 \rho_{rad}(\omega_{fi}).$$

The typical form for this rate is obtained by defining the incident light in terms of the irradiance per unit frequency interval (W m^{-2} Hz^{-1}), $I(v)$. If we then note that,

$$\frac{\rho_{rad}(\omega) d\omega}{2\pi} = \frac{I(v) dv}{c}$$

we get,

$$\Gamma_{total} = \frac{1}{6\varepsilon_0 \hbar^2 c} \mu_{fi}^2 (3\gamma^2) I(v_{fi}).$$

When we are considering the absorption of unpolarized light, or absorption by an ensemble of randomly oriented molecules, then one should take an orientational average of γ^2, in which case $\gamma^2 = 1/3$, and we have,

$$\Gamma_{total}^{\uparrow} = \frac{1}{6\varepsilon_0 \hbar^2 c} \mu_{fi}^2 I(v_{fi}) = \frac{A}{c} \mu_{fi}^2 I(v_{fi}).$$

where,

$$A = \frac{1}{6\varepsilon_0 \hbar^2}.$$

We obtain the rate of emission from Einstein's argument that at equilibrium the rates of emission and absorption due to the field should yield a radiation field consistent with the Planck distribution. This allows us to relate the absorption coefficient A to the emission rate as follows,

$$\Gamma^{\downarrow}_{total} = \left[\frac{8\pi h\nu^3_{fi}}{c^3}\right] A\mu^2_{fi} = \frac{\omega^3_{fi}}{3\varepsilon_0 \pi\hbar c^3}\mu^2_{fi}$$

where we note that the emitted radiation will be oriented along the transition dipole of the molecule (however, in an ensemble of randomly oriented molecules, the emission will obviously be randomly polarized). Since the transition rate is constant in time, the emission signal from an ensemble of many simultaneously excited molecules has an exponential decay with a lifetime, τ_{rad}, given by $\left(\Gamma^{\downarrow}_{total}\right)^{-1}$. This lifetime is the so-called radiative lifetime of the state.

1.5 The Effect of Nuclear Excitations

To this point we have not explicitly discussed excitations of the nuclear wavefunction. However, when describing absorption and emission, we saw from the Franck-Condon principle that absorption initially creates a non-equilibrium nuclear state, as does emission. Such non-equilibrium states imply nuclear excitations of some kind, even for a system at T=0. Therefore, we can conclude that nuclear excitations play an important role in understanding the properties of excitons, regardless of the system or experimental conditions.

These excitations are referred to collectively as phonons, and we can understand the sense of vibrational phonons by recognizing that each bond in a molecule can be thought of as a spring. Therefore the displacement of a single atom from its equilibrium position introduces potential energy into the molecule. Once the system is allowed to develop from this state, the displaced atom will be accelerated back towards its equilibrium position, but by virtue of the restoring force being spring-like, it will overshoot and proceed to vibrate back and forth. This vibration will continue so long as the energy of the vibration is not lost or transferred somewhere else. Phonons can also describe the rotation of the entire molecule about it's center of mass, with energy corresponding to kinetic energy of rotation. For a large molecule, there are many different phonon modes. In general, the rotational phonons have much smaller energies than the

vibrational phonons, which themselves have much smaller energies than the electronic excitations.

As noted above, even when considering absorption and emission from molecular states without phonons, we end up generating a phonon (or collection of phonons) along with the electronic transition. We can also consider the possibility of exciton creation or annihilation for states with arbitrary phonon excitations, in which case, it becomes possible to absorb or emit a photon over a range of energies. In fact, it is the presence of phonon modes that broadens emission spectra around the fundamental emission energy, and likewise for absorption, at non-zero temperatures. Since the wavefunction overlap determines the absorption and emission transfer rates, it is also worth pointing out that the presence of excitations in the nuclear wavefunction (of either the final or initial states) affects μ_{fi}^2, and so the rates are modified not only by the presence or absence of appropriate energy phonons, but also by the specific motion of the phonon.

It is also possible for an electrical excitation to decay directly into a phonon (or collection of phonons). The sense of this is the same as for radiative decay, in that we can calculate the transition rate so long as we can define the initial and final states. In this thesis we will not generally treat the effects of phonons directly. However, it still is important to realize that this non-radiative decay mechanism exists.

1.6 Exciton Dissociation

Besides generating photons and/or phonons, destroying an exciton can also involve dissociation, in which case we generate free charge. In short, we can imagine removing the excited electron from the molecule entirely by exciting it up to the vacuum level, in which case it becomes unbound. We are then left with a free electron and positively charged molecule.

This can occur spontaneously from high energy phonons (i.e. large thermal energy), or as a result of an applied electric field. Classically we can understand this in terms of the electron-hole picture of an exciton. The external field will tend to drive the electron and hole apart, and if the field is sufficiently large, the two will become unbound, in which case the electron leaves the molecule. In a quantum mechanical picture, the field causes a distortion of the nuclei and

electron clouds such that the excited electon's energy increases. For a sufficiently large field, the distortion will drive the excited electron's energy up beyond the vacuum level, in which case it can lower its energy by leaving the molecule behind. Excitons can also become dissociated by absorbing energy from a photon; however, that process more properly falls under the aegis of photo-ionization phenomena.

1.7 Excitons in Amorphous Solids – Modifications to Molecular Properties

To make the connection with a disordered solid state, we first consider the effect of the surrounding medium on the properties of a particular molecular exciton. The presence of the surrounding molecules, among other things, will introduce a local electric field that alters the Hamiltonian describing the molecule, and therefore alters the excitonic energy. Often one assumes that the disturbing fields do not significantly alter the charge distributions associated with the ground and excited states (i.e. $|G\rangle$ or $|E\rangle$ remain approximately unchanged); however, the interaction energy can still lead to a change in the exciton energy. We can understand this classically by observing that if the molecule has a charge density of $\rho_i(\vec{r})$ in the initial state and $\rho_f(\vec{r})$ in the final state, then the presence of a static local field corresponding to a potential of $\varphi_{loc}(\vec{r})$ will lead to a change in the transition energy of,

$$\Delta E_{fi} = \int \phi_{loc}(\vec{r})\left[\rho_f(\vec{r}) - \rho_i(\vec{r})\right] d^3r .$$

For the case of a uniform, static local field, $\vec{F}$, then if we approximate the charge distributions by their associated dipoles, $\vec{\mu}_i$ and $\vec{\mu}_f$, then this reduces to,

$$\Delta E = -\vec{F} \cdot \left(\vec{\mu}_f - \vec{\mu}_i\right).$$

In other words, so long as the dipole of the excited state is different from the ground state (as is generally the case) then the presence of a local field will alter the transition energy. If the local medium actually responds to the excitation itself, then the local fields will not be static, and a dynamic treatment must be employed. If the local fields appreciably change the charge distributions of ground and excited states, then a more accurate treatment would be necessary

which involves the recalculation of $|G\rangle$ and $|E\rangle$ in the presence of the local potential. We will further discuss the issue of local field effects on excitons in the second section of this thesis.

In addition to local field effects, the surrounding medium will also change the distribution of phonon modes. New modes may be introduced, which if well-coupled to the exciton state will increase the likelihood that the exciton will be destroyed non-radiatively. Some modes may even be destroyed due to the loss of steric freedoms, as in the case of rotational modes in most solids. The surrounding medium will also lower the energy barrier to exciton dissociation, because in the gas phase such dissociation would require the promotion of the electron to the vacuum level, while in the solid state, the electron (or hole) need only overcome the barrier for exciting an appropriate charged state on one of the neighboring molecules.

Finally, the surrounding medium can alter the intrinsic lifetime of the exciton. This can occur in two ways. Recalling our expression for the rate of emissive relaxation,

$$\Gamma_{total}^{\downarrow} = \frac{\omega_{fi}^3}{3\varepsilon_0 \pi \hbar c^3} \mu_{fi}^2$$

we see essentially two parameters that could vary, ω_{fi} and μ_{fi}. As discussed above, local field effects can change the emission energy, and so clearly ω_{fi} can change. In addition, if the local fields are strong enough, they can substantially alter the molecular wavefunctions, and so clearly μ_{fi} can change as well. (The transition rate associated with absorption can be similarly altered, only in that case only μ_{fi} appears in the rate expression.)

1.8 Excitons in Amorphous Solids – Ensemble Effects and Energy Transfer

While certainly it is critical to understand how an individual exciton is affected by the surrounding medium, this is not sufficient to fully understand excitons in the solid state. We must also note that by placing two molecules in very close proximity to each other, we make possible the transfer of an exciton from one molecule to another, by two different mechanisms: Forster energy transfer and Dexter energy transfer. Forster energy transfer involves the resonant interaction between the dipoles of the two molecules involved in the transfer process [10]. The

expression for the Forster transfer rate between these two molecules (called the donor and the acceptor respectively) is given by,

$$\Gamma_F = \frac{1}{\tau_{rad}} \frac{1}{R^6} \left[\kappa^2 \frac{3}{4\pi} \int \frac{c^4}{\omega^4 n^4} S_D(\omega) \sigma_A(\omega) d\omega \right]$$

where τ_{rad} is the radiative lifetime of the donor, R is the distance between the two donor and acceptor molecules, n is the index of refraction of the medium, $S_D(\omega)$ is the normalized fluorescence emission spectrum of the donor molecule, $\sigma_A(\omega)$ is the normalized acceptor absorption cross section in units of cm^2, and κ^2 is an orientational term equal to,

$$\kappa^2 = \frac{3}{2} \left[\vec{\mu}_D \cdot \vec{\mu}_A - 3 \left(\vec{\mu}_D \cdot \vec{R} \right) \left(\vec{\mu}_A \cdot \vec{R} \right) \right].$$

Often the Forster transfer rate is written as,

$$\Gamma_F = \frac{1}{\tau_{rad}} \left(\frac{R_F}{R} \right)^6$$

where

$$R_F^6 = \frac{3}{4\pi} \kappa^2 \int \frac{c^4}{\omega^4 n^4} S_D(\omega) \sigma_A(\omega) d\omega .$$

The parameter R_F is known as the Forster radius, and describes the distance at which two molecules can be separated for an exciton on one to be just as likely to emit as to energy transfer to the other.

Sometimes it is simpler to deal with an expression for the Forster transfer rate which employs the observed radiative lifetime, instead of the actual (or "natural") radiative lifetime. The observed radiative lifetime, τ, is related to the natural radiative lifetime, τ_{rad}, by,

$$\tau = \eta \tau_{rad}$$

where η is the fluorescence quantum yield of the molecule. Therefore, we can define an effective Forster radius, $\widetilde{R}_F$, such that,

$$\Gamma_F = \frac{1}{\tau} \left(\frac{\widetilde{R}_F}{R} \right)^6$$

and,

$$\tilde{R}_F^6 = \frac{3}{4\pi}\kappa^2\eta_D \int \frac{c^4}{\omega^4 n^4} F_D(\omega)\sigma_A(\omega)d\omega$$

where η_D is the fluorescence quantum yield of the donor.

Dexter transfer involves the correlated tunneling of the excited electron and hole from one molecule to another [11]. As a result, the rate of Dexter transfer is directly dependant on the overlap between the HOMO and LUMO wavefunctions of the initial and final molecules. However, the transfer rate is often given simply as,

$$\Gamma_D = \hbar P^2 e^{-2r/L} \int F_D(\omega)\sigma_A(\omega)d\omega$$

where P and L are parameters not easily related to experimental values. The sense of this form is simply that, first, the rate is proportional to the donor emission – acceptor absorption overlap and, second, it falls off exponentially with distance because wavefunction overlap falls off approximately exponentially with distance. We will not discuss Dexter transfer further in this thesis, and therefore forgo a more detailed discussion of this mechanism.

In addition to energy transfer, when understanding excitons in solids we also want to understand the aggregate behavior of collections of molecules and excitons in a single sample (which represents the bulk of practical systems in organic optoelectronics). The primary issue is that in such systems the bulk behavior represents an ensemble average over all the individual excitons. Above we outlined how the local medium might alter an individual exciton's properties, and for amorphous solids, each of the local mediums is theoretically different. Therefore, to treat such results, we need to consider distribution functions for the different properties. In theory, we would need distributions to describe the exciton absorption and emission energies and both transition rates. Depending on the specific mechanism one proposed to explain the origin of the various changes in energy and rate, these distributions might even be coupled.

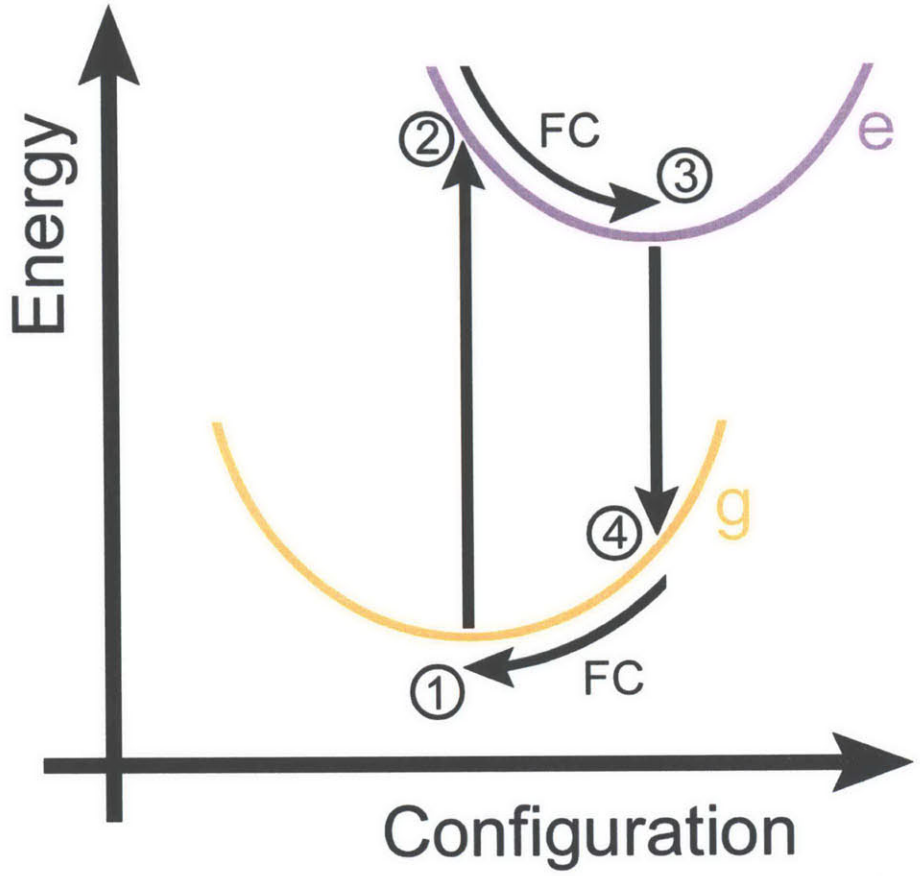

Figure 1.1 Energy-Configuration diagram illustrating the Franck-Condon (FC) shift. The vertical lines correspond to the electronic transitions from the ground (g) electronic state to the excited (e) electronic state. These are the 1-2 and 3-4 transitions. Following each transition, the system equilibrates to the new charge distribution, attaining it's lowest energy configuration. These are the 2-3 and 4-1 transitions.

2. SOLID STATE SOLVATION

2.1 Background

The work presented in this section has grown out of two recent reports by Bulovic *et al* describing spectral red shifts in the emission of amorphous organic thin films doped with the red laser dye DCM2 [12,13] (see Fig. 2.1 for chemical structures). By changing the concentration of DCM2 present in a film of N,N'-diphenyl-N,N'-bis(3-methylphenyl)-[1,1'-biphenyl]-4,4'-diamine (TPD) from 0.9% to 11%, the peak electroluminescence emission wavelength was shifted from λ=570 nm to λ=645 nm (see Fig. 2.2). (For these measurements, the DCM2:TPD film comprised the active layer of an OLED.) Because DCM2 is a highly polar molecule (with μ~11 D in ground state), and TPD is nearly nonpolar (with μ~1 D in ground state), increasing the DCM2 concentration increases the strength of the local electric fields present in the film. This increase in the local fields was associated with the spectral shift. Similar results were also observed for DCM2 in Alq_3. A subsequent report argued that the spectral shift is actually due to a progressive increase in the presence of clustered dye molecules with increasing dye concentration [14]. In this case, the authors studied the electroluminescence of DCM2 in an OLED structure, and saw that increasing the DCM2 concentration was correlated to a decrease in the quantum efficiency of the device, which they attributed to the presence of an increase in the prevalence of aggregated dye molecules (see Fig. 2.3). Since aggregated dye molecules are generally thought to have red-shifted emission compared to the monomer, these authors correlated the red shift in photoluminescence of Alq_3:DCM2 films to the decrease in electroluminescent quantum efficiency as the DCM2 doping was increased, and concluded that red shifts simply reflected an increase in emission from aggregate states. We set out to clarify this issue, by developing an experiment that isolated the "solid-state solvation" effect described by Bulovic.

2.2 Photoluminescence of PS:CA:DCM2 Films

We performed photoluminescence measurements (using λ=480 nm light) on films consisting of a polystyrene (PS) matrix, a small concentration of the laser dye DCM2, and a range of concentrations of the polar small molecule material camphoric anhydride (CA). (In these films, only the DCM2 molecules fluoresce upon excitation by λ=480 nm light). The films were spun cast at 2000 rpm from solutions with a total concentration of 30 mg/mL. The solutions were all made by first massing out polystyrene into a vial and then adding appropriate amounts of 20 mg/mL CA solution and 0.033 mg/mL DCM2 solution.

This material system was designed to allow us to keep the DCM2 concentration constant, and thereby fix DCM2 aggregation effects, while still modifying the dipole concentration of the film. We modified the dipole concentration by changing the concentration of CA, which has a large dipole moment (μ~6D in ground state) relative to its molecular weight and is essentially optically inactive over the range of wavelengths relevant for studying the properties of DCM2. The polymer host material polystyrene was chosen because it provides a transparent, non-polar background for the system.

For a fixed DCM2 concentration of 0.005%, the DCM2 emission spectrum shifts continuously from 2.20 eV (563 nm) to 2.05 eV (605 nm) for CA concentrations ranging from 0% to 24.5% (see Figs. 2.4 and 2.5). (Chemical structures of CA and PS are shown in Figure 2.4.) These results show that large shifts in emission spectra can be observed in films that have negligible DCM2 aggregation. Furthermore, the spectral shift is clearly correlated with the increase in the concentration of polar molecules in the amorphous host thin film. While these results already make it difficult to support a theory that these spectral shifts involve the aggregation of DCM2 molecules, we also performed the same experiments with DCM2 concentrations up to 0.05%, and observed no change, again indicating that the concentration of DCM2, and therefore aggregation effects, do not contribute to the spectral shifts (at least for the low level DCM2 concentrations employed.)

These results would then tend to suggest a "solid state solvation" effect like the one presented by Bulovic. However, in that report, the physical mechanism for the spectral shifts is described only generally, in that it is related to the presence of significant local fields in the medium and that the local fields are due to the presence of dipolar molecules. We agree with

this assessment, so far as it goes, but it is necessary to take this analysis further if we are to evaluate quantitatively if such a mechanism makes sense.

2.3 Theory of Spectral Shifts due to Local Fields

As discussed in Section 1.6, the presence of local fields can modify the energy associated with a molecular transition. In this section we further develop the theory of the changes in the transition energy between an initial state $|i\rangle$ and a final state $|f\rangle$, where these wavefunctions correspond to the molecule in the presence of zero field. In general, the changes to the transition energy come from two sources.

The first source comes from a direct modification by the local field of $|i\rangle$ and $|f\rangle$, which implies a modification of the associated E_i and E_f. If we describe the exact states and energies in the presence of the field by $|\tilde{i}\rangle$, $|\tilde{f}\rangle$, $\tilde{E}_i$, and $\tilde{E}_f$, then the change in the transition energy due to this internal modification of the electronic structure, ΔE_{int}, is given by,

$$\Delta E_{\text{int}} = (E_f - E_i) - (\tilde{E}_f - \tilde{E}_i).$$

To determine the exact energies, $\tilde{E}_i$ and $\tilde{E}_f$, it is generally necessary to perform a full quantum mechanical calculation of the molecular energy levels in the presence of the field. Clearly this is not very desirable, because it makes it almost impossible to develop a straightforward relationship between the external field and the change in transition energy. We will return to this difficulty below.

The second source comes from the electrostatic interaction between the molecular charge distributions of the initial and final states and the local field itself. This is the type of energy shift mentioned in Section 1.6. As indicated there, the change in the transition energy is just given by the difference between the electrostatic interaction energies in the two states (although in that expression a static local field was assumed, which is not the case here). If we identify the change in the transition energy due to electrostatic interactions by ΔE_{es}, then we have,

$$\Delta E_{es} = \int [\varphi_f^{loc}(\vec{r})\rho_f(\vec{r}) - \varphi_i^{loc}(\vec{r})\rho_i(\vec{r})] d^3r$$

where $\varphi_i^{loc}(\vec{r})$ and $\varphi_f^{loc}(\vec{r})$ describe the potentials due to the local fields for the two states, and $\rho_i(\vec{r})$ and $\rho_f(\vec{r})$ are the charge distributions for the two states. In a more complete treatment, one would determine the electrostatic interaction energies using the charge distributions due to $|\tilde{i}\rangle$ and $|\tilde{f}\rangle$, but to simplify the analysis, we assume that $|i\rangle$ and $|f\rangle$ are unaffected by the presence of a local field. This allows us to use the $\rho_i(\vec{r})$ and $\rho_f(\vec{r})$ computed for an isolated molecule. In addition, we know that $\Delta E_{\text{int}} = 0$, and so we only have to determine ΔE_{es}.

To do this, we first obtain a simpler form for the charge distributions. For excitons, we are dealing with neutral molecules, in which case the dominant term of the multipolar expansion of $\rho(\vec{r})$ is the dipole moment. If we work within this dipole approximation, and note that the electrostatic interaction energy between a dipole, $\vec{\mu}$, and an electric field, $\vec{F}$, is,

$$E = -\vec{\mu} \cdot \vec{F}$$

then we have that,

$$\Delta E_{es} = -\left(\vec{F}_f \cdot \vec{\mu}_f - \vec{F}_i \cdot \vec{\mu}_i\right)$$

where $\vec{\mu}_i$ and $\vec{\mu}_f$ are just the dipoles associated with $\rho_i(\vec{r})$ and $\rho_f(\vec{r})$. Now all that remains (within our approximations) is to determine $\vec{F}_i$ and $\vec{F}_f$.

The first (and most straightforward) treatment of this problem is attributed to Onsager, who can be thought of as the originator to the continuum approximation. In short, Onsager recognized that one way to treat the field due to a collection of surrounding molecules was to lump the surrounding molecules into a continuous medium characterized by a single parameter, the dielectric constant, ε. In the Onsager model, therefore, the surrounding molecules form a homogeneous dielectric.

Since it is necessary to define a boundary between the medium and the molecule under study, Onsager proposed that the molecule exists within a spherical cavity of radius a, and that the charge distribution due to the molecule, in the dipole approximation, consists of an appropriate point dipole located at the center of the cavity. In this model, the surrounding medium produces an electric field *in response* to the presence of a charge distribution in the

cavity (because the "medium" is just a dielectric), and for this reason, the resulting field is known as the reaction field. For a dipole of $\vec{\mu}$ we find that the reaction field, $\vec{F}_R$, is given by,

$$\vec{F}_R = \frac{\Lambda}{a^3}\vec{\mu}$$

where

$$\Lambda = \frac{2(\varepsilon - 1)}{2\varepsilon + 1}.$$

To illustrate the trends expected in $\vec{F}_R$ as ε changes, a plot of Λ over a range of ε values is shown in Figure 2.6. Note how the rise in Λ is steepest when ε is smallest, indicated that even small changes in ε can yield large changes in $\vec{F}_R$ if ε is moderately small to begin with.

In solutions, the solvent molecules are relatively free to move and reorient, and the simple dielectric description applies very well (in that the molecules typically have no intrinsic orientation, and freely rearrange themselves in the presence of a field). As a result, Ooshika, Lippert, and Mataga [15-17] subsequently applied the Onsager model to explain the shifts in absorption and emission spectra of dye molecules in solution. To follow their development we recall again the energy diagram used to explain the Franck-Condon shift, in Fig. 1.1. We recall that the difference between the absorption and emission energies is due to electronic transitions occuring much more quickly than the nuclear reorganization, and so the electronic transition occurs within a fixed nuclear framework. However, while nuclear reorganizations might be slow relative to electronic transitions, they are still fast compared to exciton lifetimes.

Now consider expanding our picture of the "system" to include the surrounding medium. In addition to the nuclear response to an electronic transition, we now have to consider a response (due to the surrounding medium) to the change in the charge distribution on the molecule under study. If this response is to include molecular rearrangements, then clearly it must occur on a time scale slow compared to electronic transitions. It might even occur on a time scale slow compared to exciton relaxation, which would create a rather complicated problem. However, measurements have shown that typically the solvent response is still fast compared to the exciton lifetime. As a result, the reaction field due to the surrounding medium, just like the nuclear framework of the molecule itself, is fixed during an electronic transition.

However, since equilibrium can be achieved during the lifetime of the exciton, we assume the absorption and emission processes to occur from the equilibrium states.

Figure 2.7 showns a new energy diagram which indicates the four different states of the molecule required for computing the absorption and emission energies, now including the solvation shift along with the Franck-Condon shift. Because this theory was originally developed for solutions, the energy shifts are referred to as solvation shifts (or sometimes, solvatochromic shifts). To compute the magnitude of the energy shift due to solvation, ΔE_{solv}, for emission and absorption, we note that the dipole and reaction field present in each of the four states is given by,

$$1:\ \vec{\mu} = \vec{\mu}_g,\ \vec{F} = \frac{\Lambda}{a^3}\vec{\mu}_g,\ E_{solv} = -\frac{\Lambda}{a^3}\mu_g^2$$

$$2:\ \vec{\mu} = \vec{\mu}_e,\ \vec{F} = \frac{\Lambda}{a^3}\vec{\mu}_g,\ E_{solv} = -\frac{\Lambda}{a^3}\left(\vec{\mu}_e \cdot \vec{\mu}_g\right)$$

$$3:\ \vec{\mu} = \vec{\mu}_e,\ \vec{F} = \frac{\Lambda}{a^3}\vec{\mu}_e,\ E_{solv} = -\frac{\Lambda}{a^3}\mu_e^2$$

$$4:\ \vec{\mu} = \vec{\mu}_g,\ \vec{F} = \frac{\Lambda}{a^3}\vec{\mu}_e,\ E_{solv} = -\frac{\Lambda}{a^3}\left(\vec{\mu}_e \cdot \vec{\mu}_g\right)$$

and so,

$$\Delta E_{solv}^{\uparrow} = -\frac{1}{a^3}\Delta\vec{\mu} \cdot \left(\Lambda\vec{\mu}_g\right)$$

$$\Delta E_{solv}^{\downarrow} = -\frac{1}{a^3}\Delta\vec{\mu} \cdot \left(\Lambda\vec{\mu}_e\right)$$

where the up and down arrows refer to absorption and emission respectively. The critical point to observe here is that for a given molecule, every term in the shift is constant except for Λ. Therefore, for different solvents, the spectral shift should always be proportional to Λ. Indeed, it has been found that spectral shifts are proportional to Λ for a broad range of polar dyes and solvents.

Nevertheless, one important refinement is necessary. In arguing that the entire response of the surrounding medium is slow compared to the electronic excitation, we were actually making an approximation that is not valid in general. Every molecule has a so-called electronic polarization response, characterized by the molecule's electronic polarizibility, α_{el}, which

describes the capability of a molecule to change it's dipole moment in response to a field by modifying its electron orbitals. In the simplest case, if we include the electronic polarization response, we have that,

$$\vec{\mu} = \vec{\mu}_0 + \alpha_{el}\vec{F}$$

where $\vec{\mu}_0$ is the dipole of a molecule in zero field, $\vec{\mu}$ is the dipole in the presence of a field $\vec{F}$. Our solvent comprises a collection of molecules that are all in principle capable of electronic polarization, and as a result, are capable of a response on the same time scale as the electronic transition itself. Therefore, to properly treat an electronic transition in such a medium, we need to somehow differentiate this fast response from the total response. This is done by employing the index of refraction, n, of our medium in addition to the dielectric constant.

The index of refraction allows us to describe the component of the dielectric response of the medium due to electronic polarization because it applies to the optical time scale, which is too short to include any other kinds of response. The reaction field due to this "optically fast" response, $\vec{F}_R^{op}$, is given by,

$$\vec{F}_R^{op} = \frac{\Lambda_{op}}{a^3}\vec{\mu}$$

where,

$$\Lambda_{op} = \frac{2\left(n^2-1\right)}{2n^2+1}.$$

Incorporating the optically fast response of the medium into our development gives us the following new results for the four different states,

$$1:\ \vec{\mu} = \vec{\mu}_g,\ \vec{F} = \frac{\Lambda}{a^3}\vec{\mu}_g,\ E_{solv} = -\frac{\Lambda}{a^3}\mu_g^2$$

$$2:\ \vec{\mu} = \vec{\mu}_e,\ \vec{F} = \frac{\Lambda}{a^3}\vec{\mu}_g + \frac{\Lambda_{op}}{a^3}\left(\vec{\mu}_e - \vec{\mu}_g\right),\ E_{solv} = -\frac{\Lambda}{a^3}\left(\vec{\mu}_e \cdot \vec{\mu}_g\right) - \frac{\Lambda_{op}}{a^3}\left(\vec{\mu}_e - \vec{\mu}_g\right)\cdot\vec{\mu}_e$$

$$3:\ \vec{\mu} = \vec{\mu}_e,\ \vec{F} = \frac{\Lambda}{a^3}\vec{\mu}_e,\ E_{solv} = -\frac{\Lambda}{a^3}\mu_e^2$$

$$4:\ \vec{\mu} = \vec{\mu}_g,\ \vec{F} = \frac{\Lambda}{a^3}\vec{\mu}_e + \frac{\Lambda_{op}}{a^3}\left(\vec{\mu}_g - \vec{\mu}_e\right),\ E_{solv} = -\frac{\Lambda}{a^3}\left(\vec{\mu}_e \cdot \vec{\mu}_g\right) - \frac{\Lambda_{op}}{a^3}\left(\vec{\mu}_g - \vec{\mu}_e\right)\cdot\vec{\mu}_g$$

and so,

$$\Delta E_{solv}^{\uparrow} = -\frac{1}{a^3}\Delta\vec{\mu}\cdot\left(\Lambda\vec{\mu}_g - \Lambda_{op}\vec{\mu}_e\right)$$

$$\Delta E_{solv}^{\downarrow} = -\frac{1}{a^3}\Delta\vec{\mu}\cdot\left(\Lambda\vec{\mu}_e + \Lambda_{op}\vec{\mu}_g\right).$$

This allows us to compute the spectral shifts due to solvation from a knowledge of the charge distributions and size of the isolated molecule and from the bulk dielectric constant and index of refraction of our medium. In practice, however, this theory is more useful for predicting the trends in the spectral shifts with ε and n than for directly computing the shifts themselves, in large part because the spherical cavity approximation is rather imprecise, making the proper choice for a hard to determine from first principles.

As indicated above, this theory works quite well for predicting the trends in spectral shifts in solutions. Since we can similarly measure an ε and n for our solid films, we should be able to straightforwardly apply the same theory to our data. Indeed, it should be pointed out that the solvation theory applies to *any* system in which a dielectric response can be identified. However, there are additional considerations in a solid sample. In particular, in a solid, the individual molecules would not be expected to have as much steric freedom as the molecules in a solution. This implies that unlike in a solution, in a solid the medium could support permanent local fields. For a particular molecule, this would mean that in addition to the solvation spectral shift, there would be a shift, ΔE_{static}, due to the presence of a static field, $\vec{F}$, given by,

$$\Delta E_{static} = -\vec{F}\cdot\Delta\vec{\mu}.$$

If these fields are random, as one might expect to be the case in a completely amorphous solid, then after averaging over all the molecules in the film, there should be no net shift in either the absorption or emission spectra. (Depending on the magnitude of the shifts, however, one might observe a broadening of the spectra, due the dispersion in the absorption and emission energies that such fields would produce.) However, if the fields are somehow correlated, then it is possible for them to produce an overall shift. There is at least one obvious form such correlation might take.

We have said that *once formed* the molecules in a solid are generally not capable of significant reorientation. However, during formation, the molecules in the film may have substantial orientational freedom. For spun films, we observe that while still in solution, the

molecules are clearly free to move around, and presumably become progressively less free as the solvent evaporates and the molecules come out of solution during the spinning process. If the film formation is not too abrupt, such a process would be expected to yield a film that has achieved a fair degree of local equilibrium. Similarly, for an evaporated film, since the film is formed extremely slowly (e.g. a few mono-layers a minute) and the molecules have fairly high kinetic energy upon deposition, each molecule should be able to establish a reasonable local equilibrium. Thus, while we describe our films as being amorphous, we must admit the possibility of local order corresponding to the attainment of some kind of local equilibrium.

Within the Onsager model, we can identify the field corresponding to the maximal degree of local equilibrium from the standpoint of the molecule under study. It is simply the reaction field for state 1 from the discussion above. However, this reaction field would have been set-up while the film was in a state with a presumably much higher ε, and clearly, it is not straightforward to determine the value of that ε. Nevertheless, we keep in mind that static fields might play an important role in spectral shifts if local ordering of the molecules occurs, and that the form of the spectral shifts in that case will be such that,

$$\Delta E_{static} = -\vec{F}_R^{static} \cdot \Delta\vec{\mu}$$

for both absorption and emission, where,

$$\vec{F}_R^{static} = \frac{\Lambda}{a^3}\vec{\mu}_g$$

with ε and a in this case correspond to the film *during formation*.

There are various ways to further refine the theory presented here for treating the effect of local fields on exciton energies. As noted earlier, we have generally neglected the possibility that the local field could modify the intrinsic energy difference between the two states, and have similarly neglected the potential for the local fields to modify the charge distributions which are involved in the electrostatic energy shifts. Furthermore, the use of the dipole approximation and the spherical cavity approximation are both potentially inappropriate. All of these shortcomings are remedied by performing a self-consistent quantum mechanical calculation of the molecule within an arbitrary cavity surrounded by a dielectric, as pioneered by Tomasi et al. Moving beyond the dielectric continuum approximation altogether remains a challenge, and practically useful techniques have not yet been developed. However, we conclude by recalling that while

more accurate methods might be possible, the expressions derived above still hold very well for identifying the trends in solutions. And so we begin with those expressions for the analysis of our data, which requires a knowledge of ε and n in our films.

2.4 Dielectric Measurements of PS:CA:DCM2 Films

We performed measurements of the electronic susceptibility of our PS:CA:DCM2 films by measuring their capacitance when sandwiched between two aluminum electrodes. The bottom electrodes were 300 Å thick and deposited using the shadow mask shown in Figure 2.8 (a). The top electrodes were 500 Å thick and deposited using the shadow mask shown in Figure 2.8 (b). In each case, the metal layers were deposited by thermal evaporation at a pressure of $\sim 1 \times 10^{-6}$ torr and at a rate of ~2 Å/s. The total device area, A_D, was 2.5×10^{-6} m^2. The film thicknesses were determined by profilometry (by measuring the profile across a scratch through the film to the glass substrate). Exactly the same solutions and spin conditions were used to make these PS:CA:DCM2 films as were used in the fluorescence measurements.

The capacitances were measured at 10 KHz, 100 KHz, and 1 MHz using an HP4192A. No significant change in the capacitances was observed when changing frequencies. Above, 1MHz, the HP4192A measurements rapidly become unreliable (in part because of the presence of stray inductances in probe lines). As we discussed above, it has been found that in solutions the dielectric response generally occurs on a time scale short compared to the exciton lifetime. However, this need not be the case in solids. We can state this in a more useful way: we are only interested in dielectric response that occurs at frequencies equal to or higher than the inverse of the radiative lifetime. In the case of DCM2, the radiative lifetime is ~ 2 ns, so we are really interested only in dielectric response at frequencies of 500MHz or higher. Therefore, we have measured the susceptibility at the highest frequency for which we can obtain reliable results. While we have no reason to expect the susceptibility to change substantially between 1 MHz and 500 MHz, such a change is technically possible, and this limitation of the measurement should be kept in mind. (In nearly all liquids and most solids, however, dielectric responses are approximately constant below the GHz regime. The main exception to this is mobile ion motion, which is not present in our films.)

The film susceptibilities are plotted in Figure 2.9, and have all been calculated assuming that our device structure forms a parallel plate capacitor with a (potentially leaky) dielectric in between. (Because the HP4192A measures capacitance and conductance independently, it does not matter if the film is not perfectly insulating.) We find that the susceptibility increases markedly with increasing CA concentration, following a linear relationship given by $\varepsilon = 2.44 + 0.13\,(CA\%)$. For the calculations of ε we have assumed that both electrode interfaces are flat. This is the case for the bottom interface, however, the top interface is formed on top of the spun PS:CA:DCM2 film, and does have some roughness. In particular, profilometry measurements show approximately sinusoidal roughness with a lateral period of about 50μm and a vertical amplitude of about 1000Å peak-to-peak. All of the film thicknesses were between 2200Å and 3200Å, and accounting ε for such roughness yields a correction to ε of between 1% and 3% depending on the film. Since other experimental errors account for a larger uncertainty in ε than this correction, we have neglected it.

We also measured the index of refraction of the films, and found it varied between 1.55 and 1.65 for all of the samples. Within the error of ± 0.10, n is nearly constant. Even if the measurement error was zero, however, the total change in n (or, more appropriately, n^2) is would still quite small compared to the change in ε.

2.5 Comparison between Measurement and Theory

We now have sufficient data to compare our spectra shift in DCM2 emission in PS:CA:DCM2 films with the solvation theory presented above. We can rewrite our expression for the change in emission energy due to solvation effects such that,

$$\Delta E_{solv}^{\downarrow} = -A\Lambda - B\Lambda_{op}$$

where,

$$A = \frac{1}{a^3}\Delta\vec{\mu}\cdot\vec{\mu}_e$$

and

$$B = \frac{1}{a^3}\Delta\vec{\mu}\cdot\vec{\mu}_g .$$

As we have discussed, this level of theory is only useful for predicted trends, so we now propose a functional form for the emission energy of,

$$E^{\downarrow} = C + \Delta E^{\downarrow}_{solv}$$

where C is some constant. Because the change in the index of refraction with CA concentration is so small, we can take the Λ_{op} term as approximately constant and lump it into C, leaving us with,

$$E^{\downarrow} = C - A\Lambda$$

In Figure 2.10 we plot three different fits to the data, indicating the sensitivity of the fit to the choice of A. (No particular significance is accorded to the value of C in this treatment.) We find that the trend in the spectral shift is in excellent agreement with the solvation theory, with the optimal fit obtained for A = 0.57 eV. It is difficult to determine how reasonable this value is based on the definition for A because of the inherent arbitrariness of a and the necessity of knowing the exact ground and excited state dipole vectors. However, we can look at solvation in solutions, as within our theory DCM2 would be expected to have a similar solvation response in solutions as in solids. A plot of the peak emission energy for DCM2 in different solvents is shown in Figure 2.11 against each solvent's value for Γ. (Because n does not change much from one solvent to the other, ranging from ~1.4 up to ~1.5, we again take the Λ_{op} term to be constant.) We observe that again the solvation theory is in excellent agreement with the data (which is not surprising for a solution system) with the optimal fit obtained for A = 0.55 eV. The remarkable agreement between the two values for A makes a strong case for the solvation theory being the operating mechanism in the spectral shifts observed in PS:CA:DCM2 films. While we had cautioned that in solids one would also expect some degree of static field effects, and that it was not unreasonable to believe such static fields were correlated in such a way that they could produce spectral shifts, the fact that ε increases so much with increasing CA concentration would suggest that within the PS matrix, the CA molecules are relatively free to reorient (which would tend to reduce any static field effects). Thus it is not surprising that solvation effects to dominate in this system.

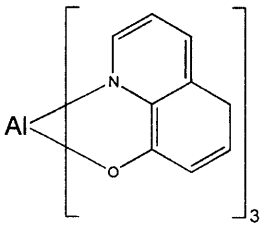

Alq_3

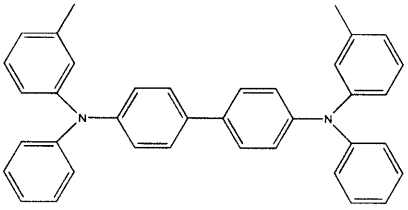

TPD

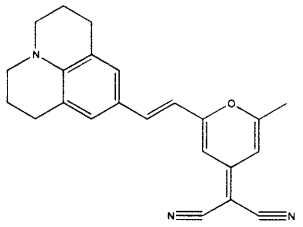

DCM2

Figure 2.1 Chemical structures of TPD, Alq_3, and DCM2.

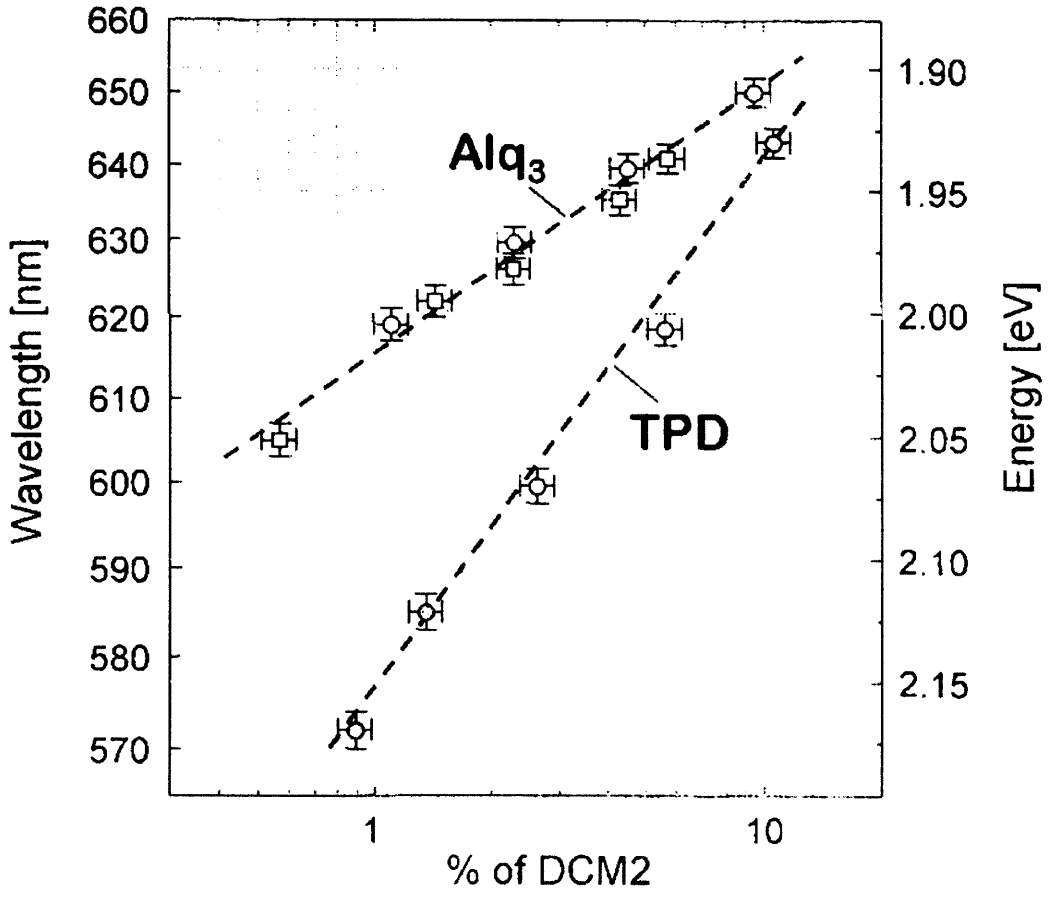

Figure 2.2 Evolution of the electroluminescence spectra of Alq_3:DCM2 and TPD:DCM2 films. For each measurement, the film DCM2 doped film comprised the active layer in an OLED. (From [13].)

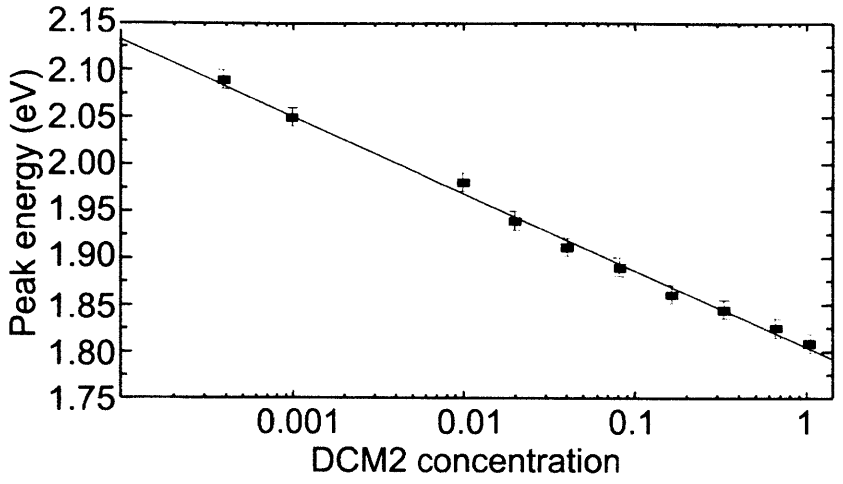

(a)

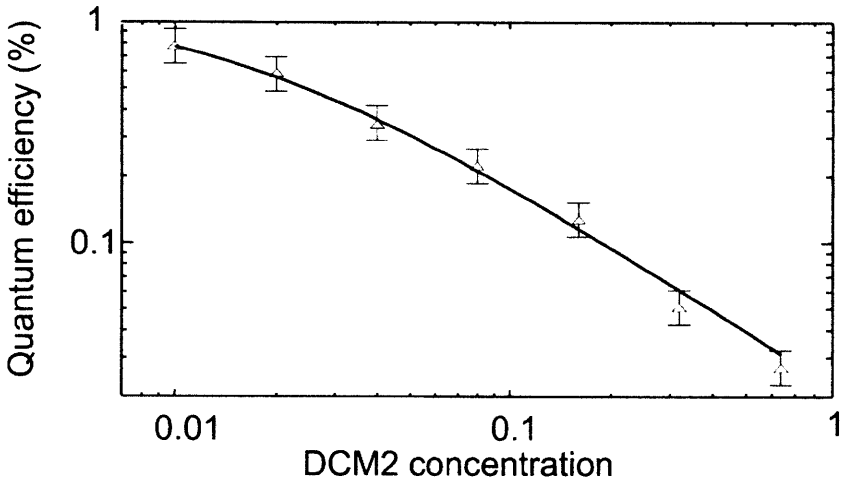

(b)

Figure 2.3 (a) Evolution of the peak photoluminescence of films of Alq_3:DCM2 with different DCM2 concentrations. (b) The evolution with DCM2 concentration of the quantum efficiency of OLEDs with Alq_3:DCM2 films as the active layer. (From [14].)

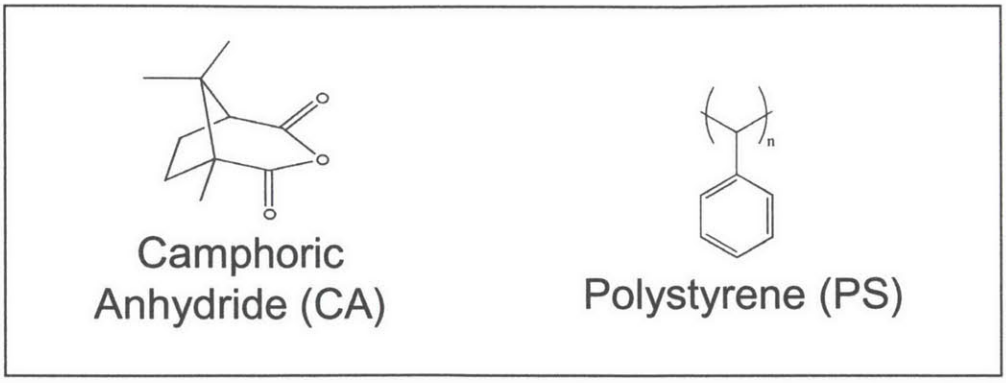

(a)

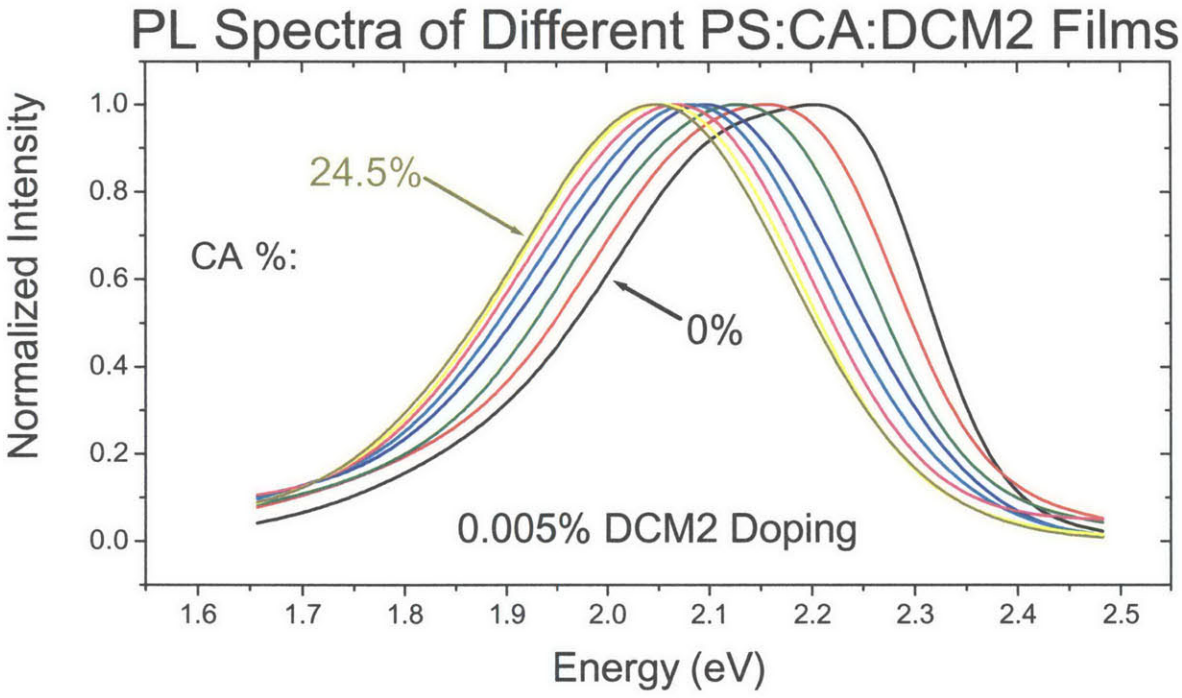

(b)

Figure 2.4 (a) Chemical structures of camphoric anhydride (CA) and polystyrene (PS). (b) Photoluminescence spectra of PS:CA:DCM2 films with different CA concentrations ranging from 0% to 24.5%. In each of the PS:CA:DCM2 films, the DCM2 concentration was 0.005% by mass.

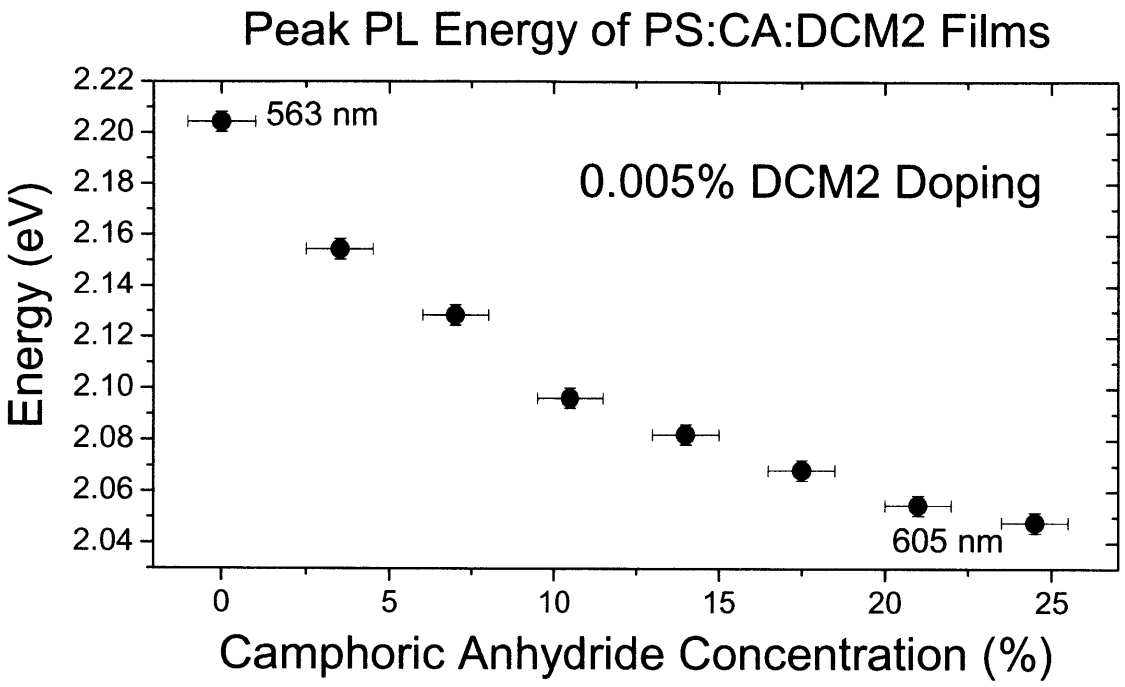

Figure 2.5 Evolution of the peak photoluminescence of PS:CA:DCM2 films with CA doping. The DCM2 doping level was fixed at 0.005%.

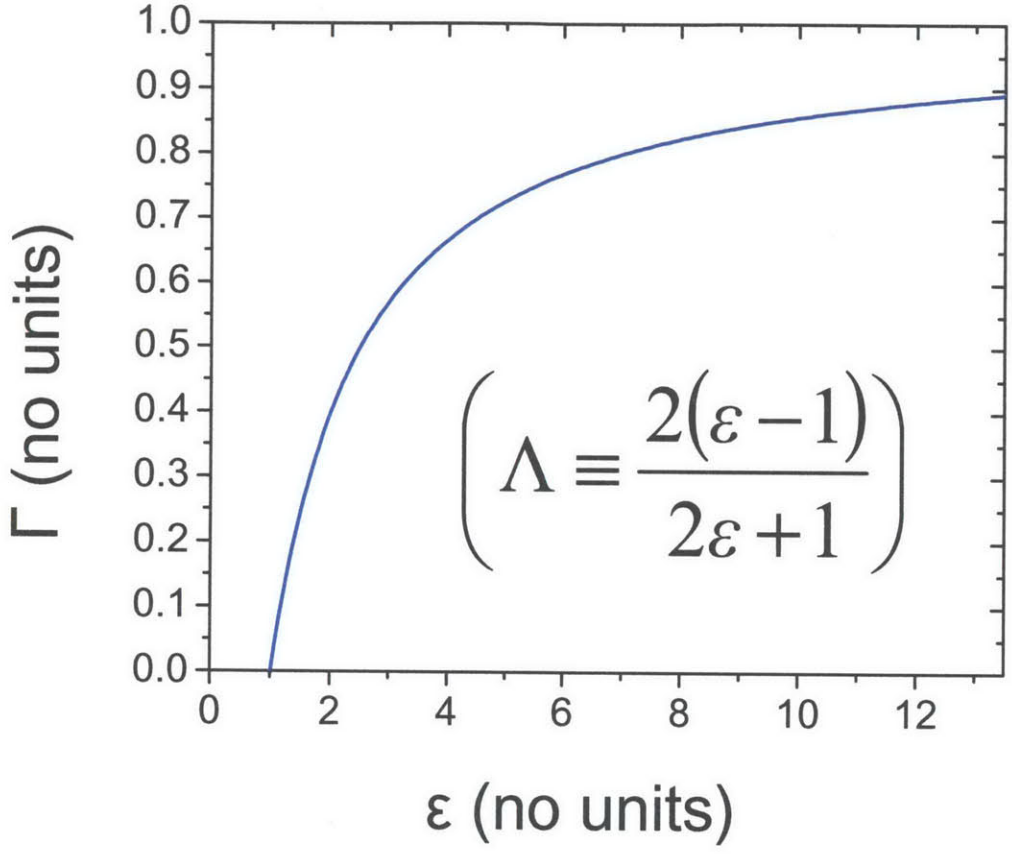

Figure 2.6 Plot of Λ as a function of ε. Note how changing ε from 1 to ~3 results in as large a change in Λ as changing ε from ~3 to ∞.

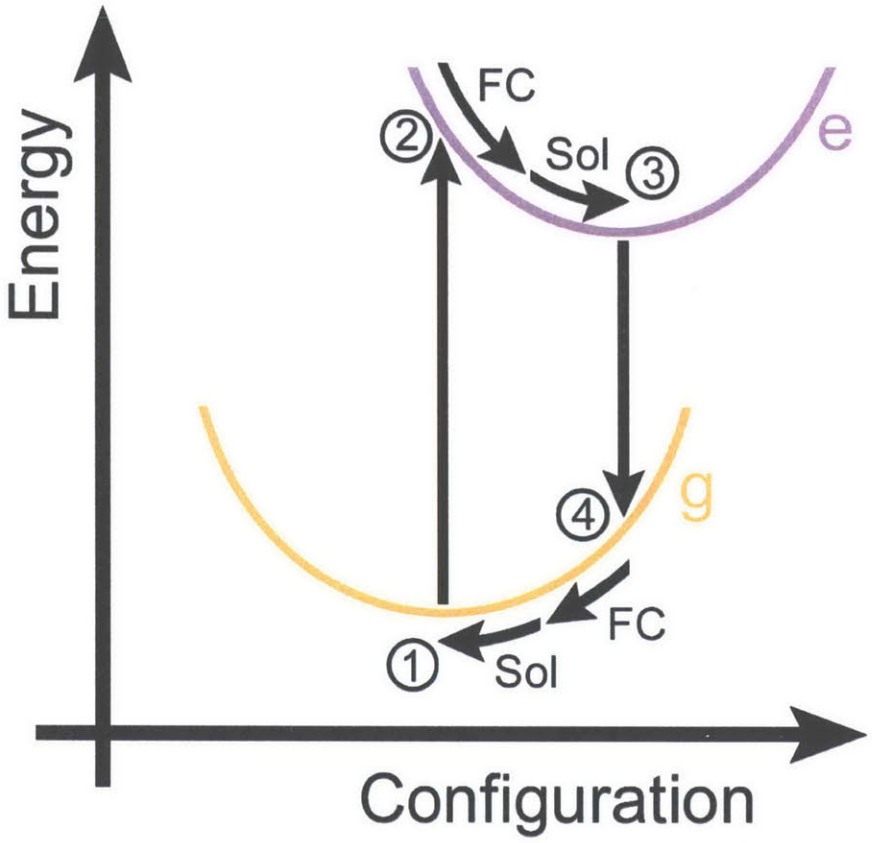

Figure 2.7 Energy-Configuration diagram illustrating the Franck-Condon (FC) and solvation (Sol) shifts. The vertical lines correspond to the electronic transitions from the ground (g) electronic state to the excited (e) electronic state. These are the 1-2 and 3-4 transitions. Following each transition, the system equilibrates to the new charge distribution via both FC and solvation responses, attaining it's lowest energy configuration. These are the 2-3 and 4-1 transitions. Note that in addition to the developing shifts shown above, implicit in the diagram is the solvation induced overall shift of the (g) and (e) curves, which could either reduce or increase the energy separation.

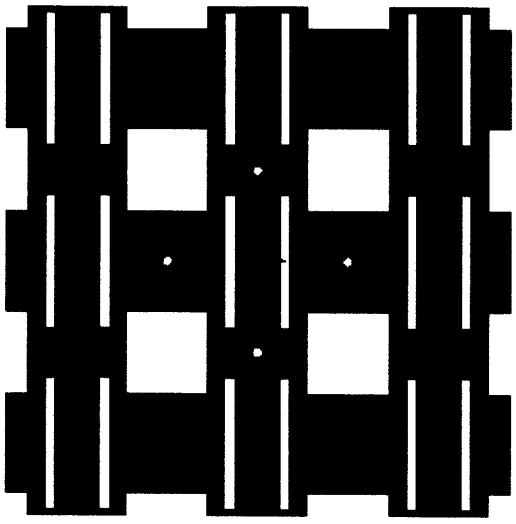

(a)

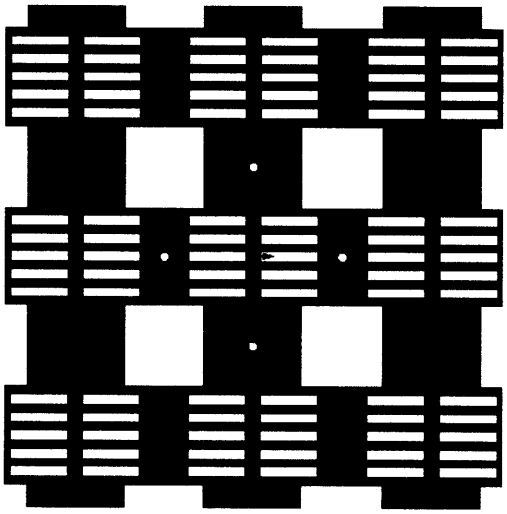

(b)

Figure 2.8 Drawings of shadow masks used to define bottom (a) and top (b) electrodes of capacitor structure used in measurements of the electronic susceptibility of PS:CA:DCM2 films.

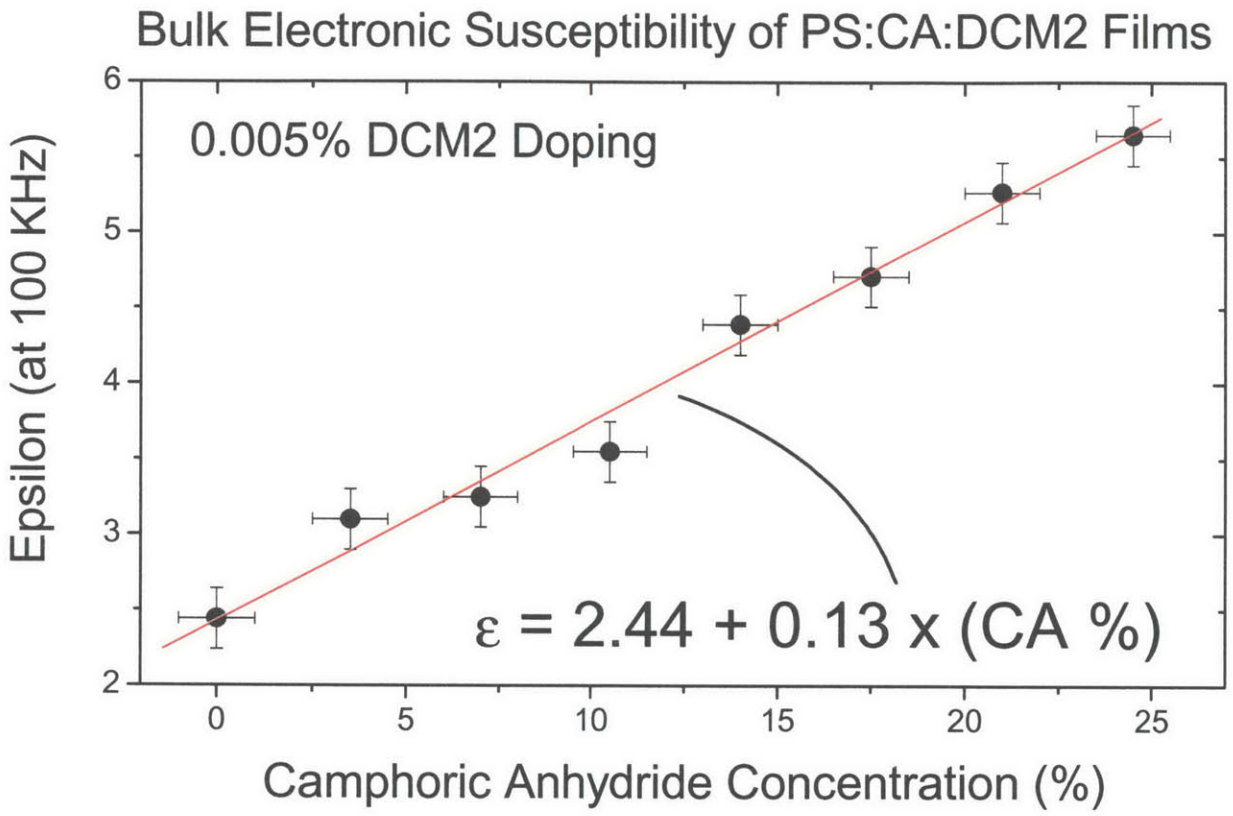

Figure 2.9 Evolution of the bulk electronic susceptibility at 100 KHz of PS:CA:DCM2 films with changing CA concentration. The DCM2 doping was 0.005% for all of the films.

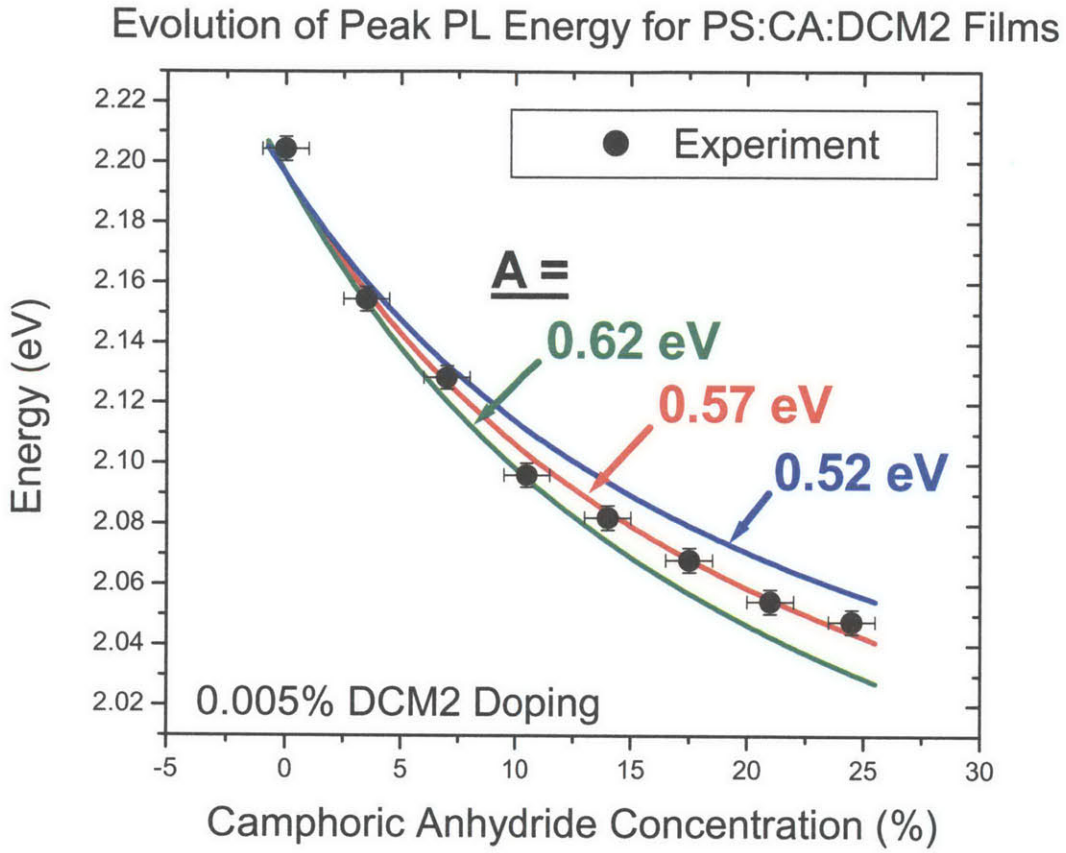

Figure 2.10 Comparison of theoretical fit using simple solvation theory and measured shifts in the photoluminescence of PS:CA:DCM2 films for different CA concentraions. The fit for three different values of A are shown, indicating the sensitivity of the fit. The best agreement with experiment was obtained for A=0.57 eV.

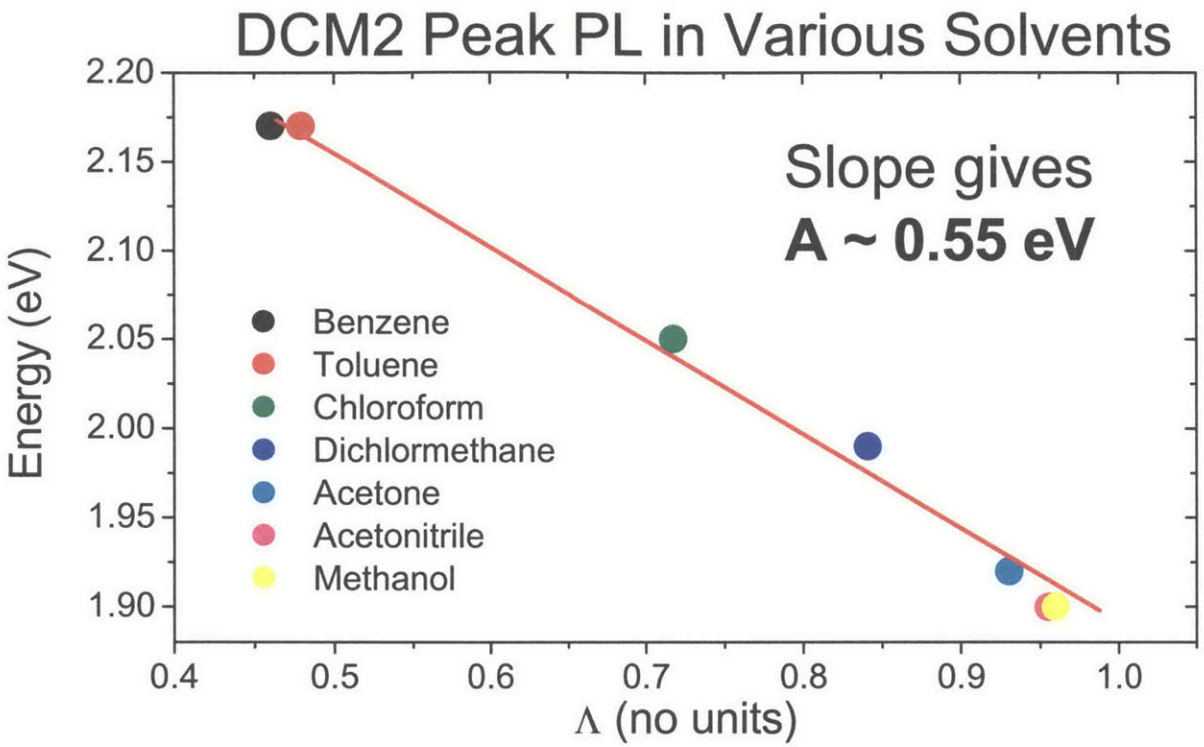

Figure 2.11 Plot of DCM2 peak photoluminescence in different solvents. When plotted against the value of Λ for each solvent, we get a straight line, with negative slope equal to 0.55 eV.

3. EXCITON DIFFUSION

3.1 Dynamic Spectral Shifts in Alq_3:DCM2 Films

We performed measurements of the time resolved photoluminescence of thin films of Alq_3 doped with the red laser dye DCM2 (with dopant concentrations ranging from between 0.5% and 10% by mass). All of our films were grown by thermal evaporation at a pressure of $\sim 1 \times 10^{-6}$ torr and at a rate of ~2Å/s. In our experiments, each film was optically excited with λ = 400 nm 100 fs laser pulses, generated by directing the mode-locked output of a Coherent Mira Optima 900 (Ti-Sapphire) laser through a BBO frequency-doubling crystal. The resulting emission signal was directed into and detected by a Hamamatsu streak camera. For all of the data presented here, a measurement time window of 5 ns was used, yielding a time resolution of ~ 10 ps.

We observed that in each film the emission spectra shifted to lower energies with increasing time, and that this trend persisted for the entire duration of the emission pulse. Selected time-resolved spectra are shown in Figure 3.1 for a 4.7% DCM2 doped sample to illustrate this shift qualitatively. The evolution of the peak emission energy with time for all the samples is shown in Figure 3.2.

3.2 Interaction between Excitation Pulse and Alq_3:DCM2 Film

To understand the physical mechanism underlying the observed spectral shifts, we must first clarify how the excitation pulse interacts with our sample. The laser pulse initially excites both Alq_3 and DCM2 molecules. However, Forster energy transfer from Alq_3 to DCM2 occurs extremely quickly (due to the large overlap between the DCM2 absorption and Alq_3 emission spectra), and within the first few ps all the Alq_3 excitons transfer to nearby DCM2 sites. This is confirmed by the absence of any Alq_3 emission, even when performing the measurement with a 1ns window, where our time resolution is down to 2 ps. In addition, we have performed our measurements using pulses of λ = 490 nm light (to which Alq_3 is essentially transparent) and

observed exactly the same dynamic spectral behavior, though with lower intensity responce, due to the reduced absorbtivity of the film at this wavelength.

Since the incident photons and Alq_3 excitons both have far more energy than required to excite the DCM2 singlet exciton, we must assume that there is no significant energy preference in the excitation of DCM2 sites (irregardless of how the excitation occurred). Therefore we conclude that by the time we begin detecting our emission signal with the streak camera, we have a system of DCM2 sites that have been randomly populated with excitons. This defines the starting state of our film.

3.3 Exciton Diffusion and Spectral Shifts

As indicated by the discussion in Section 1.8, since our Alq_3:DCM2 film is amorphous, each DCM2 molecule observes a different local environment. This should lead a distribution of exciton energies. Once we recognize the presence of a distribution of exciton energies on our DCM2 sites, then it becomes clear how energy transfer might lead to spectral shifts over time.

In short, we argue that the dynamic spectral response observed in the Alq_3:DCM2 system is a side-effect of exciton diffusion by Forster energy transfer between DCM2 sites. In the simplest picture, Forster transfer only occurs when the final site has energy equal to or less than the initial site energy. (Strictly speaking, transfer to higher energy sites is possible, just much less likely. This is further discussed below) By virtue of there being a distribution of site energies, Forster energy transfer should progressively drive excitons towards the lowest energy sites in the system. Since the emission spectrum is simply a snapshot of the current exciton population in the film, then over time we should observe the emission spectrum shift to lower and lower energies.

3.4 Simulating Exciton Diffusion

While the diffusion mechanism qualitatively explains the presence of a dynamic spectral red shift, it is not immediately clear whether or not this mechanism is quantitatively consistent with the observed phenomena. To determine if this is the case, we have developed a detailed

simulation of the diffusion process with which to test our theory. In the simulation, our system consists of a collection of sites, where, in the simplest case, each site resides on a vertex of a cubic lattice. The lattice spacing corresponds to the mean inter-site spacing in an actual film. (All spatial coordinates are scaled to this value.) Each site has an exciton energy associated with it, and the ensemble average of all the site energies reproduces the excitonic density of states (DOS) of the system. This DOS is one of the required input parameters.

Once the system of sites has been created, each site is populated with an exciton, and then for each time step (of length τ_{step}), each exciton can relax, with probability τ_{step}/τ where τ is the observed radiative lifetime, or energy transfer to another site, with probability,

$$\frac{\tau_{step}}{\tau}\left(\frac{\widetilde{R}_F}{R}\right)^6$$

where $\widetilde{R}_F$ is the effective Forster radius, as defined in Section 1.7, and R is the distance between to the two sites. The τ and $\widetilde{R}_F$ values are the remaining required input parameters, where $\widetilde{R}_F$ is supplied in terms of the mean inter-site spacing. There is no energy dependence to the transition probability in our simulation, beyond forbidding transitions to higher energy sites.

We obtain τ directly from the decay profile of the total intensity of our emission pulse (which, ideally, follows a single exponential decay). We obtain the DOS by first assuming that the DOS has a gaussian shape. We then position the DOS so that it peaks at the same energy as the PL spectrum measured at the start of the emission pulse (when, as discussed above, excitons should have populated the dye sites in the film uniformly, and therefore should, as an ensemble, reflect the film's true excitonic DOS). To finalize the DOS, we must choose its width, and, along with $\widetilde{R}_F$, this is retained as a parameter for fitting the simulation results to the data.

Figure 3.3 shows the simulation results for a series of values for $\widetilde{R}_F$ ranging from 0 to 2.0 inter-site spacings. All of the simulations were run for a total time of 3 emission lifetimes, and as shown in the plot, these results are all normalized to w_{DOS} in energy and τ in time. As implied by this normalization, the dynamic spectral shift profiles have the same shape regardless of w_{DOS} and τ, and, in fact, the simulation internally works only with time units normalized to τ and energy units normalized to w_{DOS}. Besides indicating an important fundamental invariance in

the system, this also means that by simply scaling the profiles shown in Figure 3.3, the curves for any w_{DOS} and τ can be obtained.

The remaining parameter, $\widetilde{R}_F$, does not yield simulation results that are invariant under scaling, and the series of profiles is shown to illustrate the effect of modifying $\widetilde{R}_F$. In short, increasing $\widetilde{R}_F$ increases the initial slope and total magnitude of the shift. It is also worth noting, however, that for the larger values of $\widetilde{R}_F$ the shift begins to saturate, an indication that the excitons have diffused far into the low energy tail of the DOS, where there are very few available transition sites. Of course, increasing w_{DOS} also increases the magnitude of the shift (because the entire curve is scaled up proportionally). However, as we will see in the next section both parameters are sufficiently differentiated that both must be properly chosen to obtain a good fit to the measured data.

3.5 Comparison Between Simulation and Experiment

For each of the four doping levels, we achieved excellent agreement between the simulated and the measured data. In Figure 3.4 we show the data for a 4.7% DCM2 doped sample along with various simulation results. This plot illustrates the sensitivity of the simulation to changes in the input parameters, and indicates how accurately fitting the simulation to the data determines $\widetilde{R}_F$ and w_{DOS}. The simulation parameters for the optimal fit for all the samples are tabulated in Table 3.1, and the associated fits are shown in Figure 3.5.

We find that to within the error of our measurement, w_{DOS} is constant in each of the films. Unfortunately, it is not straightforward to interpret the significance of this result without knowing more about the physical mechanism that underlies the observed energy dispersion. One can argue that this result indicates that the dominant contributor to w_{DOS} is dye-host interactions, and that dye-dye interactions play only a small role (since no doping dependence was observed). However, many other factors may contribute, and even this seemingly straightforward conclusion may prove incorrect. We do, however, note that the w_{DOS} we calculate are comparable to the w_{DOS} calculated by others (e.g [18]) for conducting states in amorphous

organic materials, which we consider to be the most comparable system for which w_{DOS} values have been determined.

In addition to w_{DOS}, the fitting process also yields a measurement of $\widetilde{R}_F$ and we find that as the doping increases, $\widetilde{R}_F$ decreases, from 41 Å for the 0.5% doping level to 22 Å for the 4.7 % doping level. We argue that this trend arises from two factors: a doping dependant reduction in the absorption-emission overlap, and a doping dependant reduction in the DCM2 quantum efficiency. To understand this, we first recall from the introduction the expression for $\widetilde{R}_F$,

$$\widetilde{R}_F^6 = \frac{3}{4\pi}\kappa^2\eta_D\int\frac{c^4}{\omega^4 n^4}F_D(\omega)\sigma_A(\omega)d\omega.$$

Here we are only interested in the trends, so we drop the constants, to get,

$$\widetilde{R}_F^6 \propto \kappa^2\frac{\eta_D}{n^4}\int\frac{F_D(\omega)\sigma_A(\omega)}{\omega^4}d\omega.$$

We measured that n does not change substantially with doping for the doping levels we used. Furthermore, we expect κ^2 to be approximately constant with doping since for a fully amorphous solid state film, the average relative orientation between dye molecules is the same at all doping levels. However, as observed in our measurements, and reported elsewhere [12-14], increasing the DCM2 dye concentration substantially red shifts the emission spectrum. At the same time, we find that σ_A remains nearly unchanged with doping. As a result, as the doping level increases, the overlap integral between F_D and σ_A decreases. For the ensemble, CW spectra, the overlap integral decreases by about a factor of 6 from 0.5% to 4.7% DCM2 doping. We note that this calculation should be considered quite rough because the above overlap integral is meant to apply to the individual molecular absorption and emission spectra, while we have used the ensemble, CW spectra.

Additionally, as reported by Baldo et al [14], the quantum yield of DCM2 doped Alq_3 films decreases with increasing doping concentration. Specifically, a film doped to 0.5% should have a DCM2 quantum yield of ~ 5 times that of a 4.7% sample. Combining these effects, we find that to a first approximation one would expect a factor change of ~ 1.8 in $\widetilde{R}_F$ from 0.5% doping to 4.7% doping, which is in reasonable agreement with our calculated values for $\widetilde{R}_F$.

3.6 Simulation Refinements and their Effects

It is important to keep in mind the extent to which our treatment of exciton diffusion is approximate, and the manner in which a more sophisticated model might differ from the one presented here. In particular, in the simulation results presented above, all the DCM2 molecules are positioned precisely on lattice sites of a square lattice. This certainly does not reflect the actual distribution of DCM2 molecules in our films. Rather, one would expect the DCM2 molecules to be dispersed randomly such that on average the density corresponds to the bulk concentration but with some variations in the local densities. We can achieve this condition by allowing each DCM2 site to deviate from its "home" lattice site following a spherical Gaussian distribution. Because the Forster transfer function goes as R^{-6}, the introduction of such positional variations (which causes some neighbors to be closer than before and some farther away) leads to, on average, an increase in the aggregate rate of energy transfer. Locally, this increase can be quite dramatic, as one can see by considering a simple example. Imagine a dye site with two neighbors, each initially located 1.0 $\widetilde{R}_F$ away. The aggregate rate of transfer is then $2/\tau$. If we introduce positional variations, however, and end up with, for instance, one neighbor located 0.5 R_F away and another located 1.5 $\widetilde{R}_F$ away, then the average dye site concentration is still the same, but the aggregate rate of transfer is now,

$$\left(\left(\frac{1}{0.5}\right)^6+\left(\frac{1}{1.5}\right)^6\right)\Big/\tau = 64.1/\tau$$

a factor increase of more than 32! This example rather overstates the real effect of positional variations in our system, where the aggregate rate of transfer is averaged over many sites, some that, being far from the initial site, are only negligibly affected by the variations. Even so, it is clear that the failure to consider positional variations in a film in which they are present will cause one to compute values for $\widetilde{R}_F$ that are too large. To determine more exactly the magnitude of this potential error, we need to directly simulate the diffusion process in a system with different amounts of positional variation.

In addition to positional variations, in the fitted simulation results we have assumed that the effect of energy on the Forster transfer rate is simply to forbid transfer to a higher energy

state and allow transfer to an equal or lower energy state. It is more accurate to say that transitions to higher energy states are simply less likely than transition to lower energy states because the overlap integral will be smaller (see Figure 3.6 for a schematic illustration of this point). It is difficult to include this effect in the simulation directly without knowing the molecular absorption and emission spectra for each molecule (as noted earlier when discussing the general trends observed in $\widetilde{R}_F$.) Nevertheless, it is worth noting that if we did know those spectra, we could reimplement the simulation to compute the correct R_F for each pair of molecules. Lacking this data, however, we are constrained to make do with a single $\widetilde{R}_F$ and our simple "on" or "off" energy dependence to Forster transfer. Qualitatively, if we approximate the true energy dependence to yield a change in the overlap integral which is close to linear over the range of energies present in the system, then one would expect the primary effect of including a more accurate energy dependence to be a broadening of the spectra and little or no change in the peak evolution. As a result, it would seem reasonable to conclude that though not strictly correct, our simplified treatment of the energy dependence of the Forster transfer process should not appreciably change our results.

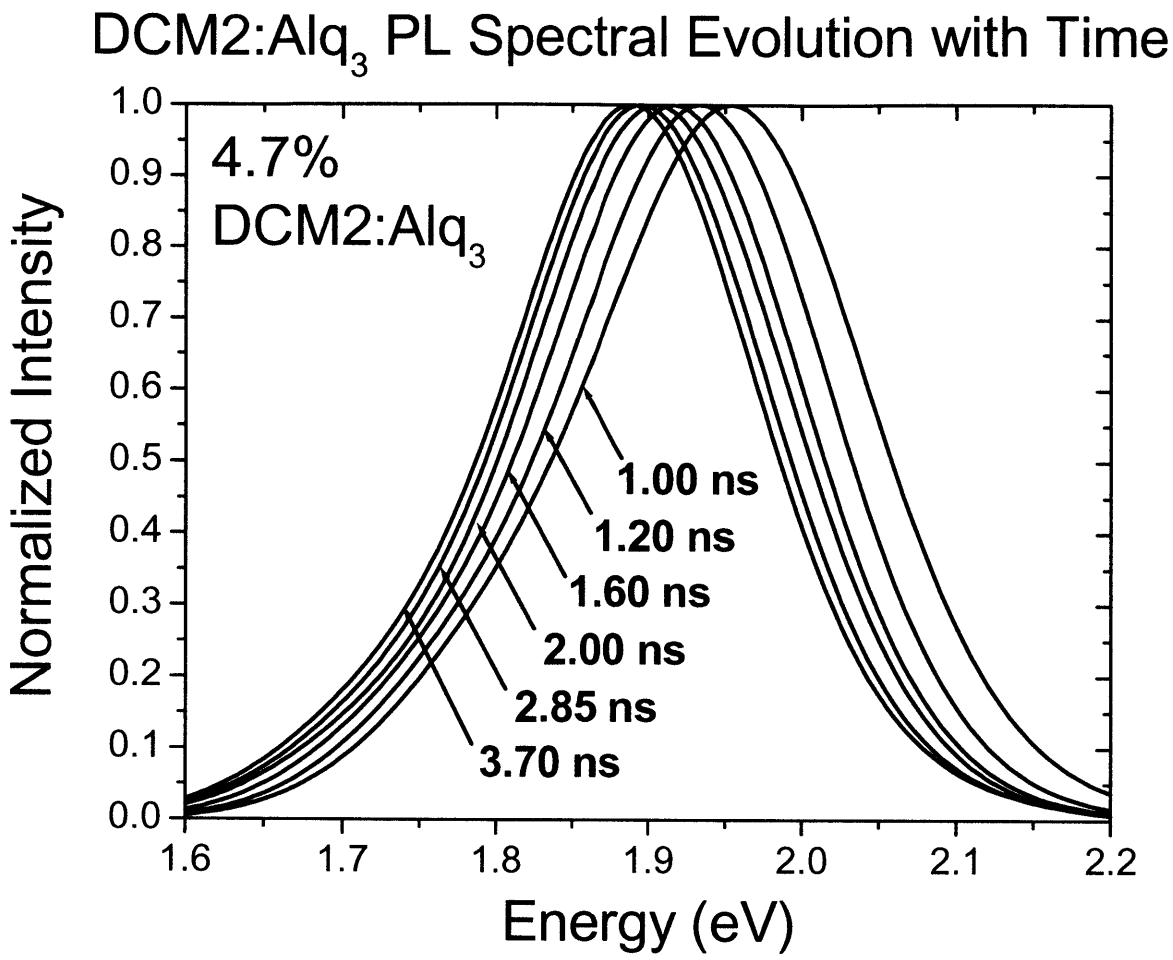

Figure 3.1 Selected normalized spectra from the time evolution of the photoluminescence of a film of Alq_3 doped with 4.7% DCM2.

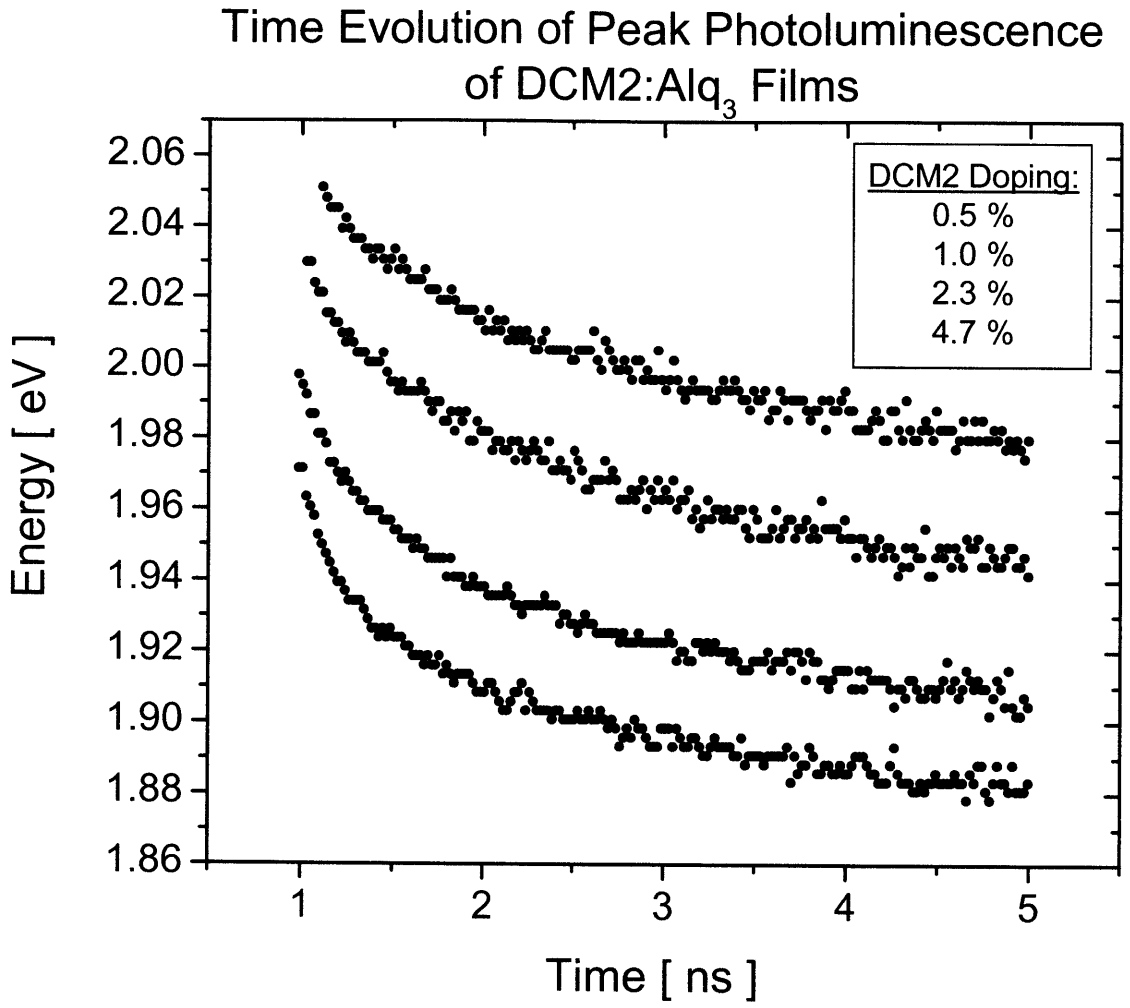

Figure 3.2 Time evolution of the peak of the photoluminescence spectra of Alq_3 films doped with different concentrations of DCM2.

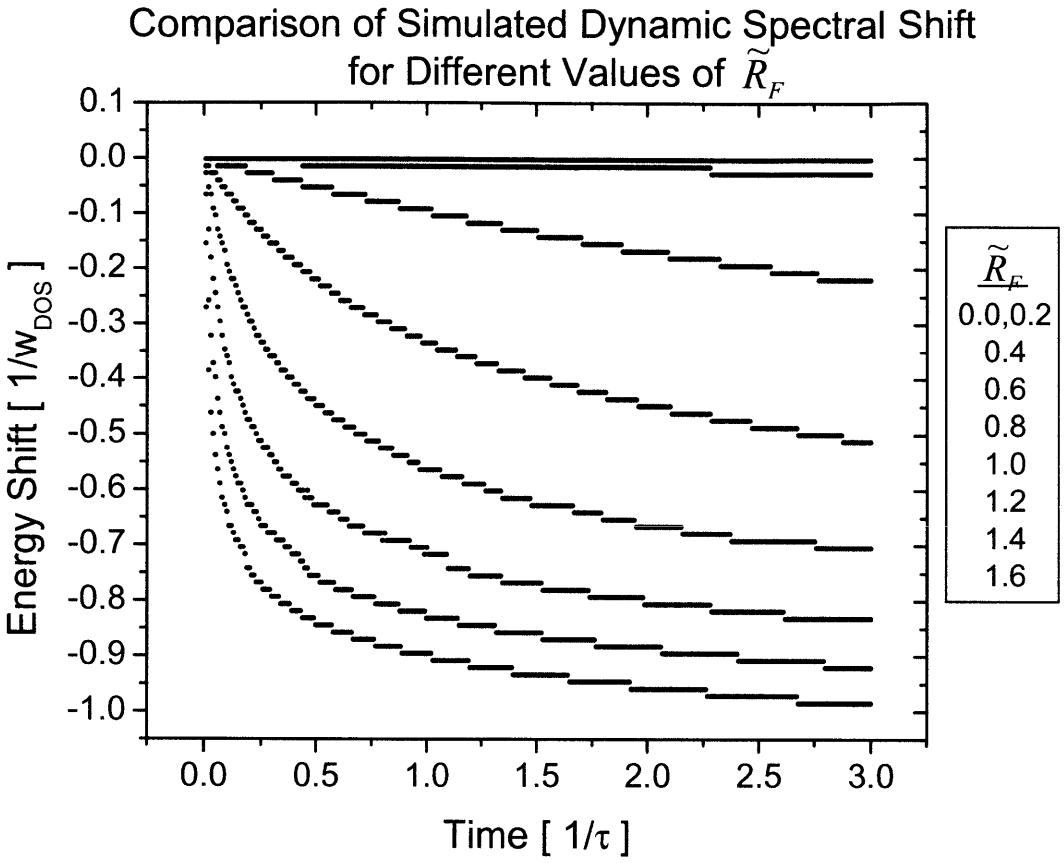

Figure 3.3 Time evolution of the peak of the simulated photoluminescence spectra for different values of the effective Forster radius. Note that the results are scaled in energy to the density of states width, w_{DOS}, and in time to the observed radiative lifetime, τ.

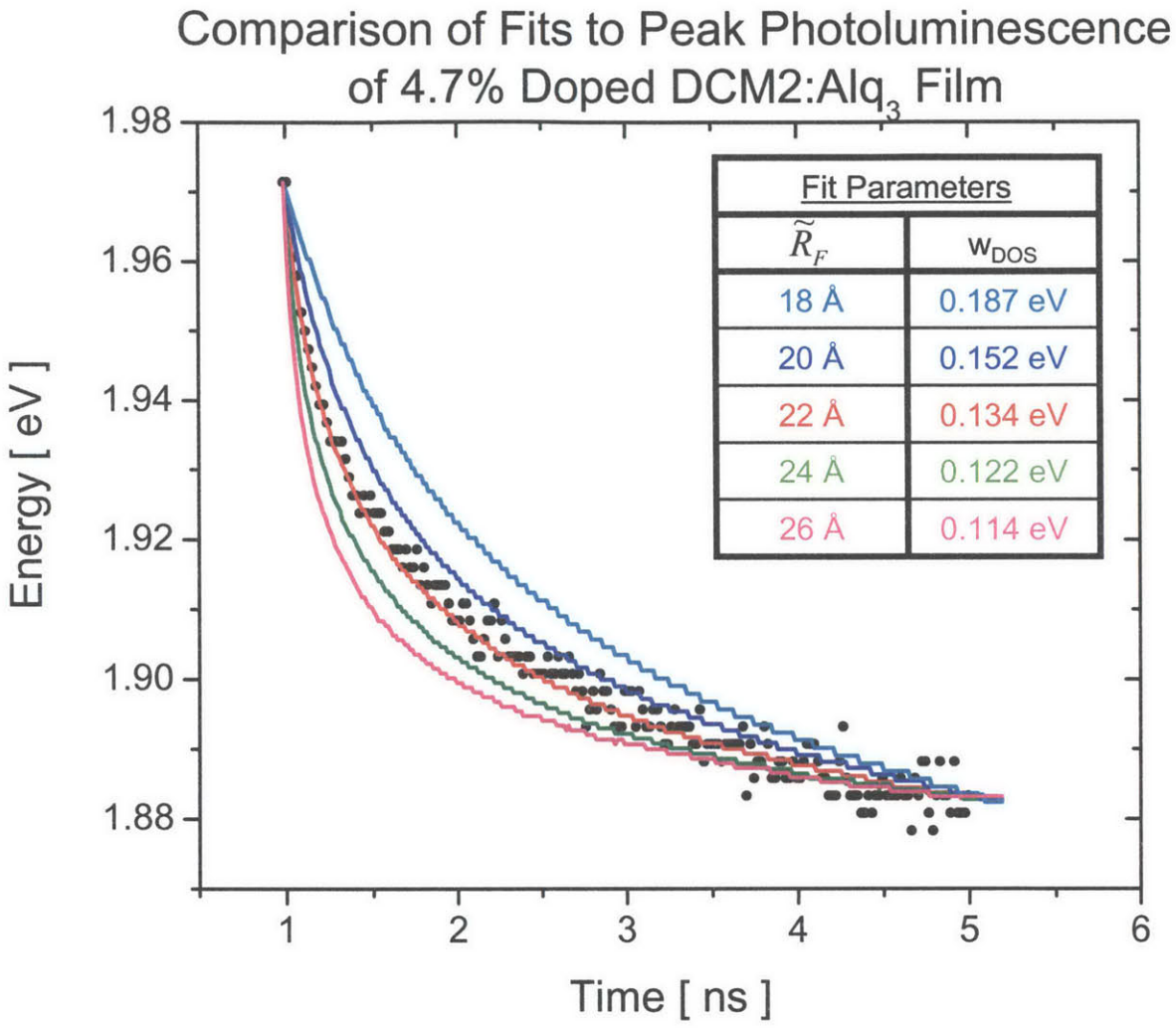

Figure 3.4 Comparison of measured and simulated results for the time evolution of the peak of the PL spectra for different values of the effective Forster radius and density of states width. In this sample, the DCM2 doping was 4.7%.

DCM2 Doping %	τ	$\widetilde{R}_F$	w_{DOS}
0.5	2.5 ns ± 0.1 ns	41 Å ± 8 Å	0.134 ± 002 eV
1.0	1.8 ns ± 0.1 ns	31 Å ± 7 Å	0.148 ± 0.02 eV
2.3	1.6 ns ± 0.1 ns	27 Å ± 5 Å	0.174 ± 0.02 eV
4.7	1.4 ns ± 0.1 ns	22 Å ± 3 Å	0.152 ± 0.02 eV

Table 3.1 Summary of optimal simulation parameters for fitting the measurements of each film. Note the marked decrease in $\widetilde{R}_F$ with increased doping, in contrast to w_{DOS}, which remains approximately constant to within our experimental errors.

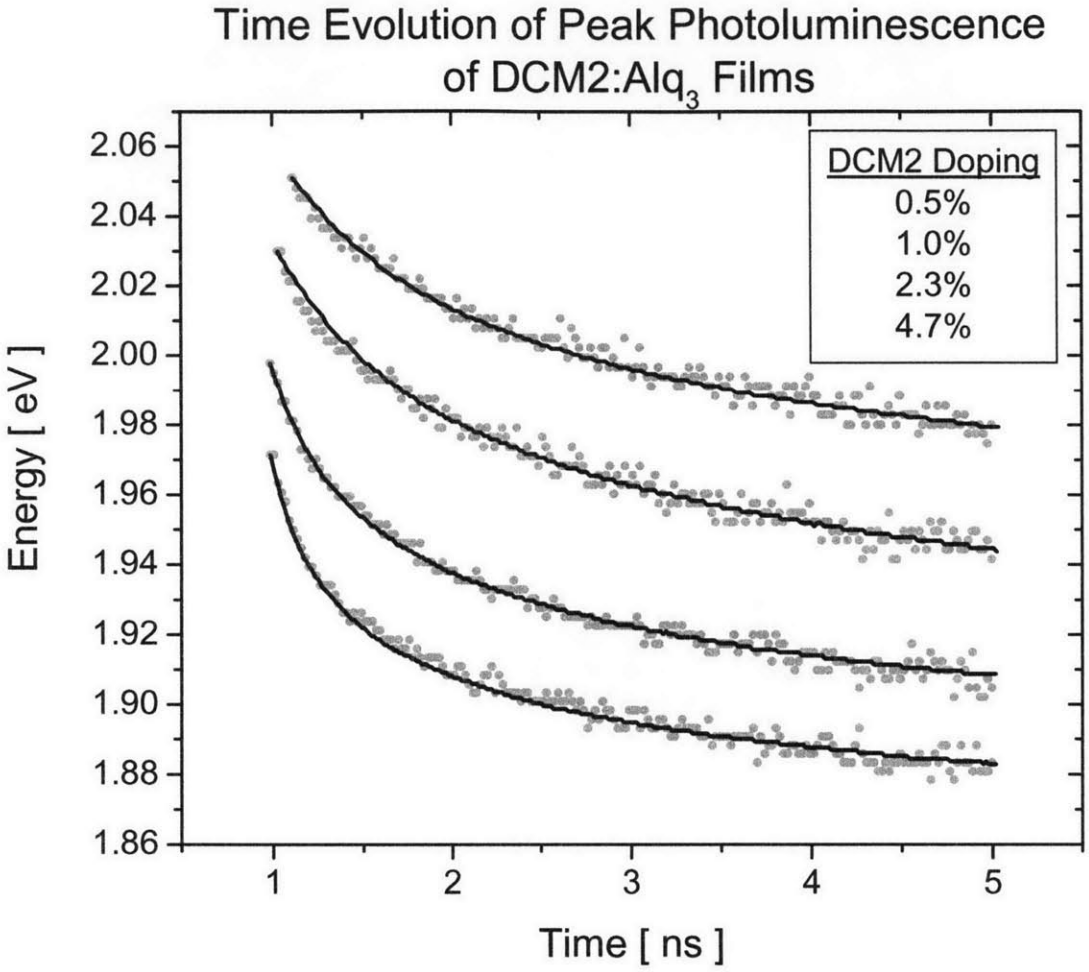

Figure 3.5 Comparison between optimal simulation fits (see parameters in Table 3.1) and measured time evolution of the peak of the PL spectra for each film.

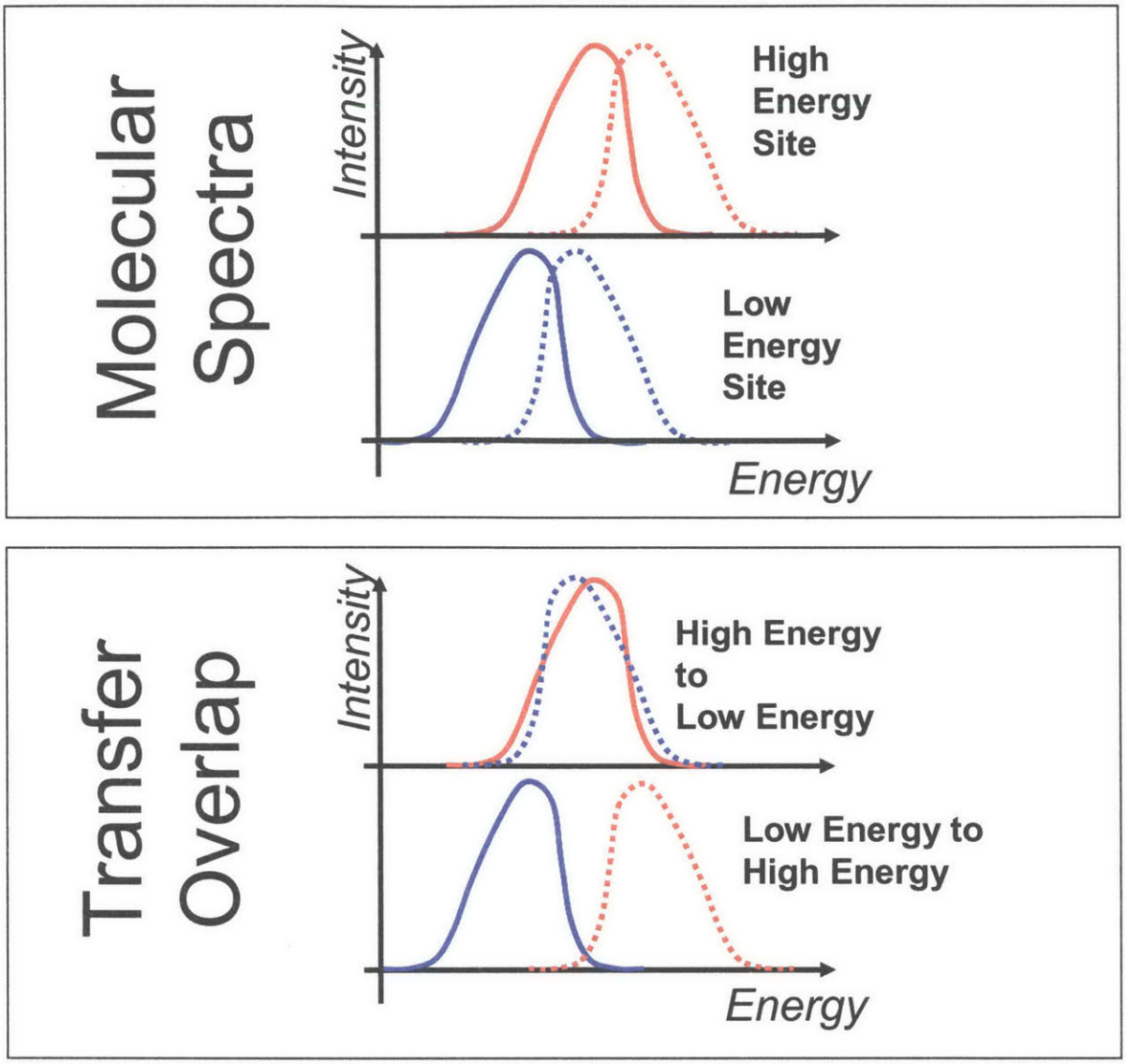

Figure 3.6 Cartoon illustrating why Forster energy transfer is more likely to occur from higher to lower energy sites than vice versa. On the top are emission (dashed lines) and absorption (solid lines) spectra for two molecules, one with "high" energy and one with "low" energy. On the bottom are overlaid the emission-absorption pairs for the two directions of energy transfer. Observe that the overlap is higher for high to low energy transfer.

4. Conclusions

4.1 Solid State Solvation

In this thesis we have presented data demonstrating a controllable shift in the emission spectra of the red laser dye DCM2 which can be attributed to the "solid state solvation" effect. The essential development of the solvation theory assumes only a dielectric response by the surrounding medium, and therefore the solid state solvation effect should be present in all amorphous organic solids (by virtue of the ε in such solids always being greater than in a vacuum). Therefore it is critical to take into account solvation effects when trying to predict the energy structure of molecules in solid films. We also described the possibility of static fields being present in the film. In the PS:CA:DCM2 system, we do not find it necessary to invoke such mechanisms, and indeed consider the marked increased in ε with CA doping as an indication of the relatively high steric mobility of the CA molecules, which would tend to limit the presence of static fields. However, this need not always be the case. Perhaps for larger dopant molecules, or for a different host, the steric freedom could be reduced, allowing for the formation of large static fields. Therefore it may be possible to produce substantial spectral shifts without any significant change in ε. Further work must be done to determine if this can be experimentally observed, and whether or not the static field mechanism can be clearly distinguished from the solvation mechanism (aside from the different ε trends).

There are a number of ways this might be accomplished. For instance, in our material system, we have used a polymer host. This was done because we wanted to use trace concentrations of DCM2 (to eliminate any DCM2 concentration effects), and therefore were constrained to spun films (where the relative concentrations are determined in solution), which are generally of higher quality for polymers than for small molecule materials. Nevertheless, it might be useful to perform the same experiments with a non-polar small molecule material like TPD, because in such a film the degree of steric freedom of the various film components might be different. To distinguish the static field shifts from the solvation shifts, we have two possibilities. First, we note that for a static field, the spectral shift is the same for absorption as for emission. On the other hand, for solvation, except in the pathological situation where,

$$\Lambda\vec{\mu}_g - \Lambda_{op}\vec{\mu}_e = \Lambda\vec{\mu}_e + \Lambda_{op}\vec{\mu}_g$$

the absorption and emission shifts are of different magnitudes. Therefore, by looking at both the absorption and emission shifts with different concentrations of dipolar dopant, one should be able to differentiate the two types of spectral shift. However, because spectral shifts may also arise from intrinsic changes in the ground and excited state wavefunctions, it may not be reasonable to assume that the emission and absorption spectra shift in lock-step the way the simple static field theory would predict. (This issue is mediated in the standard solvation theory by the fact that the theoretical relationship between the absorption and emission shifts is not directly considered. Rather, they are simply treated as two processes that can be related to ε and n, through Λ and Λ_{op}. By imposing a relationship between the two shifts, we make the test of the static field theory more stringent, and it may not continue to be valid.)

We might, however, take note of the fact that the static shift is not time dependant, and try to perform a dynamic measurement which separated the two. In a general system, we have a polarization shift (characterized by n within the solvation formalism) occurring on the same time frame as the electronic transition, followed by the Franck-Condon shift, followed by the "slow" solvation shift (characterized by ε). Practically, we can only hope to experimentally measure the dynamics of the "slow" solvation shift, but with such a measurement, we could distinguish systems with traditional solvation response and static field shifts. A time resolution in the range of 1 to 10 fs would likely be required, however, so a different approach from a streak camera would be required.

4.2 Exciton Diffusion

We have presented measurements of a dynamic spectral shift in the emission of DCM2 doped into films of Alq_3. We have shown that this phenomenon can be explained as a side effect of exciton diffusion between DCM2 sites, and that through our simulation of the process, one can obtain a measurement of the Forster radius, $\widetilde{R}_F$, and the width of the density of states, w_{DOS}. We found that w_{DOS} remains approximately constant, and that $\widetilde{R}_F$ increases with decreasing doping. We demonstrated how this trend in $\widetilde{R}_F$ is plausible, but further work must be done to

determine if this trend can be quantitatively supported. One of the methods by which this might be done would be to study films with even lower concentrations than those used here, as for concentrations below ~0.5% the quantum yield, η, of DCM2 saturates at about ~1. This should lead to a noticeable change in the trend in $\widetilde{R}_F$ as in this "very low doping" regime, only the overlap function will be changing. (Specifically, we would expect R_F to increase more slowly for the same shift in absorption and emission spectra.)

Because we argue that this phenomenon is general to systems with an appreciable w_{DOS}, measurements of other systems should be performed to determine if these results are not peculiar to the Alq_3:DCM2 system. Also, we have not explored here the physical origin of the broadening of the density of states. However, as alluded to in the introduction, there is likely a correlation with the density of dipolar molecules. This connects our diffusion work with our solid state solvation work, in that both are concerned with changes in energy structyre to local fields. However, in the solvation work we were interested in determining net shifts, while here the issue is determining the degree of energy dispersion.

One of the difficulties of the diffusion measurement, however, is that relatively large dye concentrations are required to obtain appreciable diffusion, but at the same time, in our DCM2 system, the dye concentration itself clearly has a strong effect on the DCM2 properties (as noted when discussing the spectral shifts and changes in quantum yield). We would like to work with a system in which the ground state dye molecules did not interact with one another, even in relatively large concentrations. One possible approach would be to find a dye molecule with no ground state dipole moment, but a large transition dipole moment (i.e. a large excited state dipole moment.) In that case we would not have to worry about the influence of one dye molecule on the other, but would still observe large spectral dispersion due to internal static fields. In such a system we would then controllably introduce a third material (e.g. CA) to modify the dipole concentration and thereby modify the energy dispersion. For such a measurement, it might prove useful to employ a non-polar host, like TPD, instead of Alq_3.

In addition, further work should be done to determine the specific effects of positional variations, as discussed in Section 3.6. We could trivially include such positional variations into our simulation by introducing random deviations from the lattice vertices with a uniform distribution for the angular component and a Gaussian distribution for the distance, such that,

$$P = e^{-4\log 2(r/w_{dev})^2}$$

is the normalized likelihood of deviating a distance r (in intersite spacings) from the vertex. (In this form w_{dev} corresponds to the FWHM of the Gaussian.) To avoid artifacts resulting from two molecules being anomalously close to each other (i.e. separated by less than a molecular "diameter") one would likely want to enforce a minimum separation distance. In addition to illuminating the relationship between microscopic film disorder and bulk film properties, determining the effects of such positional variations would also provide a better sense of the accuracy of our calculation of the effective Forster radius and density of states widths.

REFERENCES

[1] C. Adachi et al, *J. Appl. Phys.*, 90 (2001), 5048.
[2] P. Peumans et al, *Appl. Phys. Lett.*, 76 (2000), 2650.
[3] P. Peumans et al, *Appl. Phys. Lett.*, 76 (2000), 2855.
[4] V.G. Kozlov et al, *Nature*, 389 (1997), 362.
[5] R. Shankar, Principles of Quantum Mechanics, 2nd Ed., Plenum Press (New York), 1994.
[6] C. Cohen-Tannoudji et al, Quantum Mechanics, John Wiley and Sons (New York), 1977.
[7] P.W. Atkins et al, Molecular Quantum Mechanics, 3rd Ed., Oxford University Press (New York), 1997.
[8] A. Szabo et al, Modern Quantum Chemistry: Introduction to Advanced Electronic Structure Theory, Dover Publications, Inc. (New York), 1996.
[9] D.P. Craig et al, Molecular Quantum Electrodynamics: An Introduction to Radiation Molecule Interactions, Dover Publications, Inc. (New York), 1998.
[10] T. Forster, Modern Quantum Chemistry Part 2: Action of Light and Organic Molecules (Ed. O. Sinanoglu), Academic Press (New York), 1965.
[11] D.L. Dexter, *J. Chem. Phys.*, 21 (1953), 836.
[12] V. Bulovic et al, *Chem. Phys. Lett.*, 287 (1998), 455.
[13] V. Bulovic et al, *Chem. Phys. Lett.*, 308 (1999), 317.
[14] M.A. Baldo et al, *Chem. Phys. Lett.*, 347 (2001), 297.
[15] Y. Ooshika, *J. Phys. Soc. Japan*, 9 (1954), 594.
[16] E. Lippert, *Z. Naturforsch.*, 10a (1955), 541.
[17] N. Mataga et al, *Bull. Chem. Soc. Japan*, 29 (1956), 465.
[18] A.J. Campbell et al, *J. Appl. Phys.*, 84 (1998), 6737.